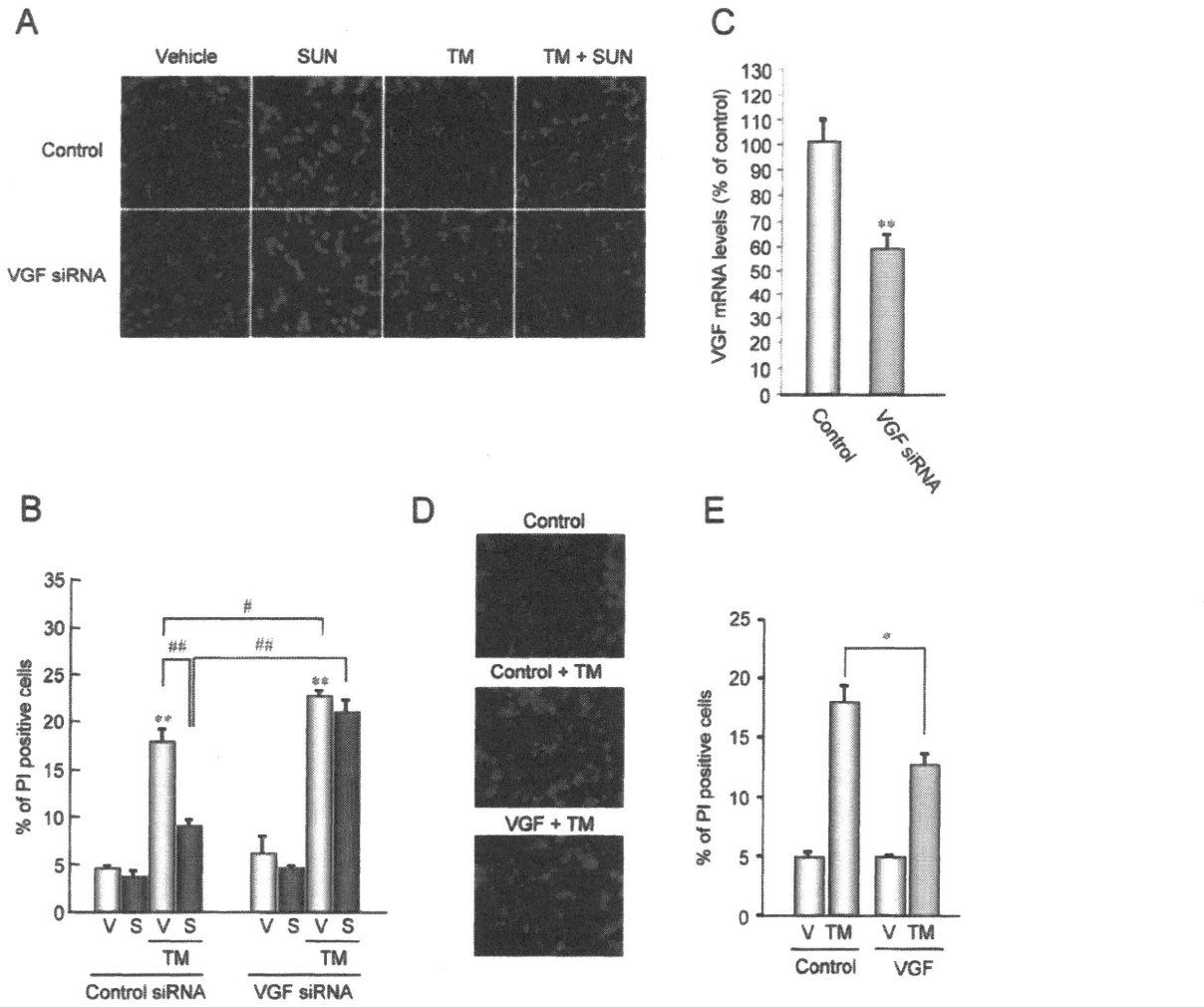

Figure 3. VGF protects cells against ER stress-induced SH-SY5Y cell death. (A) Representative fluorescence microscopy showing nuclear stainings for Hoechst 33342 (blue) and propidium iodide (green) on SHSY-5Y cells transfected VGF siRNA or control siRNA at 24 h after tunicamycin (TM) treatment with or without SUN N8075 (SUN). (B) The number of cells displaying fluorescence was counted, and positive cells were expressed as the percentage of propidium iodide to Hoechst 33342. Each column represents the mean ± S.E.M. ($n=6$). #$p<0.05$, ** and ##$p<0.01$ versus relevant control group. (C) VGF siRNA transfection reduced the VGF mRNA level in SH-SY5Y cells. Each column represents the mean ± S.E.M. ($n=6$). **$p<0.01$ versus control group. (D, E) VGF overexpression inhibited cell deathinduced by tunicamycin. *$p<0.05$ versus TM plus empty vector-transfected control control group.
doi:10.1371/journal.pone.0015307.g003

(Fig. 4E,F). In the H46R rats, the mean survival days of the vehicle-treated and SUN N8075-treated rats were 201.1±4.7 ($n=9$) and 214.7±2.0 ($n=10$), respectively (Fig. 4F, Table S4). Treatment with SUN N8075 significantly prolonged the mean lifespan by 6.7% ($p=0.012$) in the H46R rats compared with that in the vehicle-treated H46R rats. On the other hand, there was no significant difference in the course of body weight between the SUN N8075-treated and the vehicle-treated H46R rats (Fig. S6B).

In this study, SUN N8075 was administered by subcutaneous injection at 30 mg/kg for mice and at 10 mg/kg for rats, and the maximum concentrations in plasma were approximately 2 μM and 1 μM, respectively (Tamura S. et al., unpublished data). In the present study, SUN N8075 at concentrations of 1 μM or higher inhibited ER stress-induced cell death *in vitro*. Taken together, these results show that SUN N8075 could delay disease onset and prolong survival in different two types of familial ALS models.

Motor neuron loss and VGF expression in the spinal cords of G93A ALS mice and sporadic ALS patients

We evaluated the effect of SUN N8075 on motor neuron loss in the spinal cords of G93A mice at 14 weeks of age. The number of motor neurons in the lumbar anterior horn of the G93A mice was decreased to 59% of their wild-type (WT) littermates (Fig. 5A). Treatment with SUN N8075 (30 mg/kg, s.c./day) in the G93A mice significantly increased the number of surviving motor neurons compared with that in the vehicle-treated G93A mice (Fig. 5A). Recent studies revealed that a lowering VGF-derived 4.8 kDa fragment was identified in the CSF from patients with ALS [31] and that VGF content was decreased in the CSF of ALS patients and in the CSF, serum and spinal cord motor neurons of G93A mice [13]. In the present study, we used immunohistochemistry (Fig. 5B) and Western blotting (Fig. 5C) to assess the expression of the VGF protein in the spinal cord. A large number

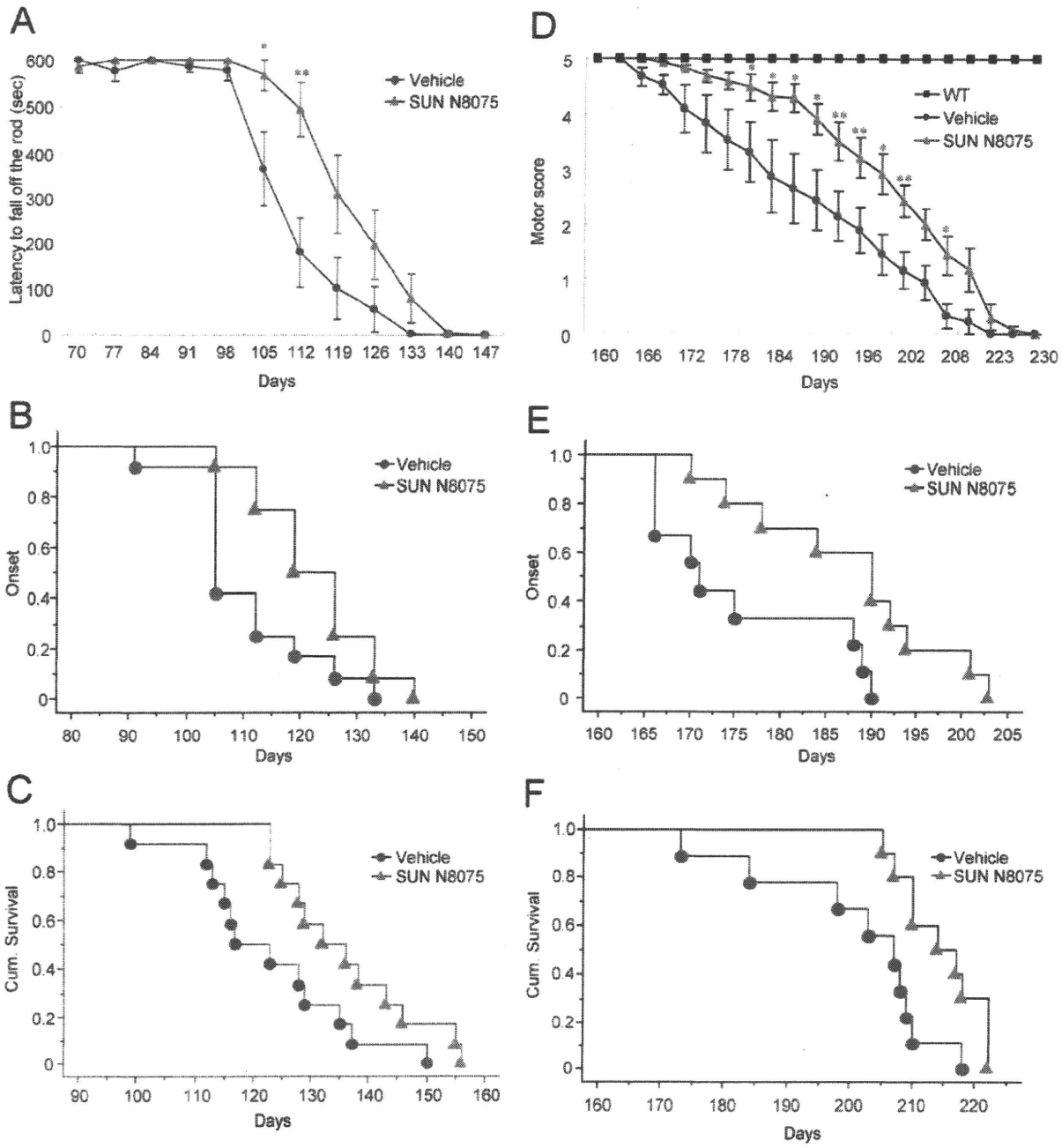

Figure 4. Effects of SUN N8075 on motor dysfunction, disease onset and survival in two types of familial ALS model animals. (A–C) G93A mutant SOD1 mice; effects of SUN N8075 at 30 mg/kg/day, s.c., on motor performance evaluated by the rotarod test (A), cumulative probability of the onset of motor deficit (B), and survival (C) in G93A mutant SOD1 mice. (D–F) H46R mutant SOD1 rats; effects of SUN N8075 at 10 mg/kg/day, s.c., on the motor performance score (D), cumulative probability of the onset of motor deficit (E), and survival (F) in H46R mutant SOD1 rats.
doi:10.1371/journal.pone.0015307.g004

of VGF-positive cells were observed in the lumbar anterior horn of the WT littermates (Fig. 5B). VGF immunoreactivity was markedly decreased in the spinal cords of GA93A mice compared with that in their WT littermates, and the reduction was significantly ameliorated by treatment with SUN N8075. Western blot analysis also revealed that a single VGF band at approximately 90 kDa was identified, and the band intensity in the spinal cord of the G93A mice was significantly decreased to 58% of that of the WT mice (Fig. 5C). Treatment with SUN N8075 inhibited the decrease in the VGF band intensity in the spinal cords of the G93A mice (Fig. 5C). Furthermore, we used double-immunofluorescent staining to determine VGF localization in the lumbar anterior horn of the spinal cord (Fig. 5D). VGF colocalized with NeuN-positive motoneuron (>25 μm diameter) but not GFAP (an

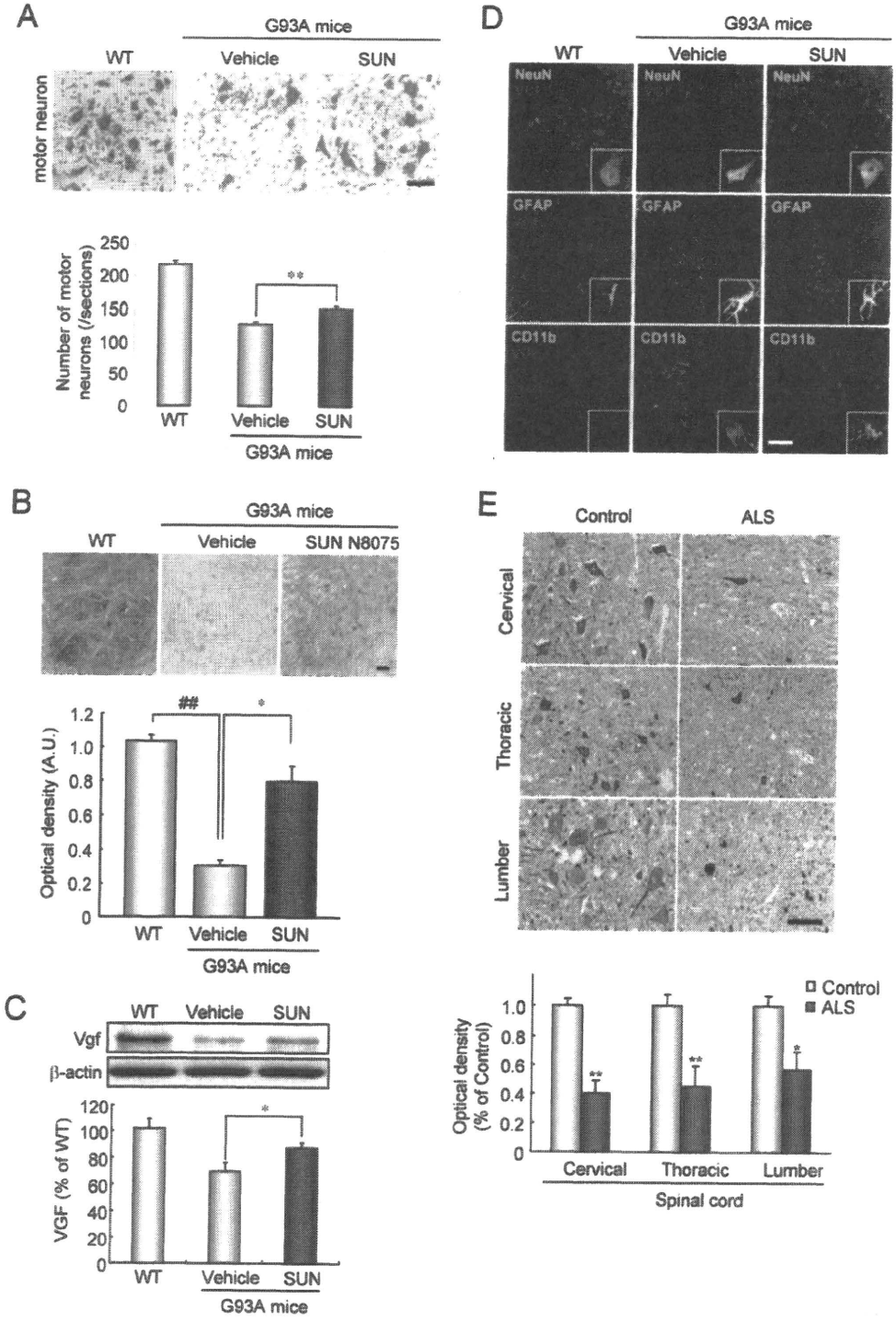

Figure 5. Effects of SUN N8075 on the decreased motor neurons and VGF immunoreactivity of the spinal cords of SOD1G93A mice and sporadic ALS patients. (A) cresyl violet staining, (B) VGF immunostaining, (C) VGF immunoblotting, and its double-immunostainings, (D) with GFAP (activated astrocyte marker), NeuN (neuronal marker) or GD11b (activated microglial marker). Scale bars = 50 μm. Each column represents the mean ± S.E.M. (n = 6). *$p<0.05$, ** and ##$p<0.01$ versus the relevant control group. (E) Human spinal cord tissue section. Representative photographs are shown for the anterior horns of the spinal cords in the control patients and the patients with sporadic ALS. Scale bar = 100 μm. Average density of VGF immunoreactivity in the anterior horn of the human spinal cord. Each column represents the mean ± S.E.M. ($n = 6$). *$p<0.05$, **$p<0.01$ versus control.

doi:10.1371/journal.pone.0015307.g005

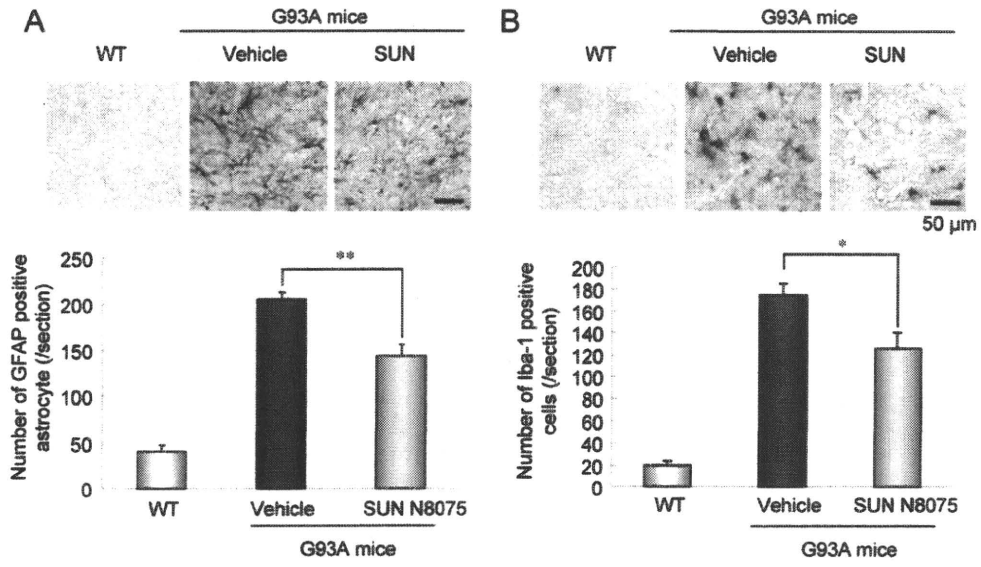

Figure 6. Effects of SUN N8075 on the glial activation in the spinal cords of SOD1G93A mice. G93A mice aged at 14 weeks-old increased the number of GFAP-positive astrocytes (*A*) and Iba-1-positive microglial cells (*B*) in spinal cord, and their increases were abolished by SUN N8075 treatment. Scale bars = 50 μm. Each column represents the mean ± S.E.M. (n = 6). *$p<0.05$, **$p<0.01$ versus WT mice.
doi:10.1371/journal.pone.0015307.g006

astrocyte marker)- or CD11b (an activated microglial marker)-positive glial cells in the lumbar anterior horn of the WT littermates (Fig. 5D). On the other hand, in the lumbar anterior horns of the G93A mice, VGF-immunoreactive signals colocalized with GFAP-positive astrocytes in addition to motor neurons but not the CD11b-positive glial cells (Fig. 5D). These data indicate that VGF expression is reduced in the spinal cords of the G93A mice, and the decrease is ameliorated by the treatment with SUN N8075. As mentioned above, the VGF level has been reported to be decreased in the CSF of ALS patients compared with normal subjects [13], but there is no evidence of the decrease in VGF in the spinal cords of ALS patients. In the present study, the expression level of VGF in postmortem spinal cords of sporadic ALS patients was markedly down-regulated, but typically expressed at high levels in the spinal cords of the control patients in any sections cervical 7 (C7), thoracic 8 (T8), and lumbar 4 (L4), respectively (Fig. 5E). The density of VGF immunoreactivity was significantly lower in the lumbar anterior horns of sporadic ALS patients than those in control patients with other diseases (0.40±0.09, 0.46±0.14, and 0.57±0.12 of the control in sections C7, T8, and L4, respectively, $n = 6$) (Fig. 5E). These data suggest that the decrease in VGF in the spinal cord is involved in ALS pathogenesis.

Gene expression profiles and glial activation in the spinal cords of G93A ALS mice

To generate gene expression profiles on the spinal cords of WT or G93A mice aged 14 weeks after SUN N8075 treatment, we performed microarray analyses on 4×44 K Agilent Mouse expression arrays. At least more than 27,000 genes out of 41,000 gene probes on the array were detected in each sample, and the Volcano plot of the probe data set averages of gene expression in the spinal cords of the G93A mice ($n = 4$) compared with the WT mice ($n = 4$) is shown in Fig. S7A. Seven hundred and twelve genes (green and red squares) were considered statistically significant between the G93A and WT mice based on the criteria of the average fold-change (FC) ≥2, p≤0.01 with the Benjamini-Hochberg correction. A heat map representation of the hierarchical clustering of the 712 different gene expressions in the spinal cords of G93A mice treated with or without SUN N8075 (each group: $n = 4$) compared with WT mice ($n = 4$) is shown in Fig. S7B. The gene expression profiles were apparent differences between SUN N8075 and vehicle treatments in the G93A mice, and a principal component analysis (PCA) component 1 discriminated significantly among the 3 groups (Fig. S7C). We analyzed the gene ontology classification for each category from the 712 different genes and listed the top 10 categories in Fig. S7D. Almost all categories included immune response genes. In particular, high intensity and variant genes (signal >1000, FC>5) were astrocyte- or microglia-related genes such as GFAP and CD11b/11c. Hence, the activation of astrocytes and microglia was determined in the spinal cords of the G93A mice using the immunohistochemical technique. The number of GFAP-positive astrocytes and Iba-1-positive microglia was significantly increased in the lumbar anterior horns of the G93A mice compared with those in their WT littermates (Fig. 6A,B). Treatment with SUN N8075 (30 mg/kg, s.c./day) significantly decreased the number of both types of glial cells in the spinal cords of the G93A mice compared with those in the vehicle-treated G93A mice (Fig. 6A,B).

Discussion

Our results showed that SUN N8075 markedly protected against ER stress-induced cell death in SH-SY5 cells at 1 μM or higher concentrations, and the protective effects are mediated by endogenous VGF production. SUN N8075 increased VGF expression as identified by microarray and secondary validation approaches. VGF synthesis is also stimulated by BDNF through ERK-dependent phosphorylation of CREB [26,27]. However, SUN N8075 did not enhance *BDNF* mRNA, suggesting that its *VGF* mRNA expression is not mediated indirectly by BDNF. On the other hand, SUN N8075 gradually increased the phosphorylation of ERK1/2 and Akt during the course of 24 h. These findings suggest that ERK-dependent phosphorylation of CREB1

and/or EGR1 upregulation may be crucial in regulating VGF gene expression by SUN N8075. Several types of VGF-derived peptides have been detected in the rat brain, bovine pituitary and human cerebrospinal fluid [32,33,34,35], and these peptides possess multiple biological activities, autonomic activation, anti-depression, enhancement in synaptic plasticity, penile erection and increases in energy expenditure [11,36,37,38]. Recently, Severini et al. [39] reported that TLQP-21, a naturally occurring VGF-derived C-terminal peptide, protects rat cerebellar granule cells against apoptosis induced by serum and K^+ deprivation, and that TLQP-21 also increased the phosphorylation levels of ERK1/2 and Akt. Furthermore, a MEK1/2 inhibitor completely attenuated the protective effect of TLQP-21 on K^+ deprivation-induced cell damage [39]. These findings support the idea that endogenous VGF induced by SUN N8075 may activate survival signals via the MEK/ERK and PI3K/Akt pathways.

A wide range of mechanisms are thought to be implicated in the pathogenesis of ALS, including mitochondrial dysfunction, excitotoxicity, oxidative stress, protein misfolding, proteosomal dysfunction, aberrant growth factor signaling, inflammatory process and glial activation [40,41]. On the other hand, the accumulated evidence indicates that ER stress plays a role in the pathogeneses of familial and sporadic ALS [4,5,6], and therefore, they may have a common mechanism for motorneuron loss through ER stress as downstream signaling pathways. In the present study, extrinsic VGF expression protected against ER stress-induced cell death in SH-SY5Y cells. Furthermore, VGF was markedly decreased in the spinal cords of the GA93A mice compared with that in their WT littermates in agreement with a previous report [13], and the reduction was significantly ameliorated by the treatment with SUN N8075. Zhao et al. [13] also reported that exogenous VGF expression by adenoviral mouse VGF transfection in the primary spinal cord neurons from SOD1 G93A mice has been reported to protect neurons against AMPA- or NMDA-mediated excitotoxic injury. Furthermore, we demonstrated for the first time that the VGF level was lower in the spinal cords of sporadic ALS patients than in the control patients. Taken together, VGF depletion may participate in disease onset and/or progression of ALS.

In conclusion, we demonstrated that SUN N8075 inhibits ER-stress-induced neuronal cell death via VGF expression and that VGF plays a critical role in motor neuron survival. Accordingly, VGF may be a potential new therapeutic target for neurodegenerative disorders, including ALS.

Supporting Information

Methods S1 Supplemental Materials and Methods for Supplemental Figures and Tables were addressed.
(PDF)

Figure S1 Anti-oxidative agents do not reveal protective effects on ER stress-induced SH-SY5Y cell death. (*A*) Edaravone at 1 to 10 μM or (*B*) *N*-acetyl-cystein (NAC) at 1 mM did not show any effects on the reduction of cell viability at 24 h after tunicamycin treatment. (*C*) Edaravone (Eda) at 10 μM, NAC at 1 mM or trolox (Tro) at 100 μM did not inhibit the reduction of cell viability at 24 h after thapsigargin treatment.
(TIF)

Figure S2 SUN N8075 and anti-oxidative agents protect cell death induced by serum devrivation, or oxidative stress in RGC-5 cells. (*A*) SUN N8075 (SUN) at 0.1 to 1 μM, edaravone (Eda) at 10 μM, and trolox at 100 μM show protective effect on the reduction of cell viability at 48 h after serum deprivation. Each column represents the mean ± S.E.M. (n = 6). ##p<0.01 versus control. **p<0.01 versus serum deprivation alone. (*B*) SUN N8075 (SUN) at 0.1 to 1 μM and trolox at 100 μM show protective effect on the reduction of cell viability at 24 h after L-buthionine-(S,R)-sulfoximine (BSO; 0.5 mM) plus glutamate (10 mM). Each column represents the mean ± S.E.M. (n = 6). ##p<0.01 versus control. **p<0.01 versus BSO plus glutamate alone.
(TIF)

Figure S3 SUN N8075 does not affect gene expression level of *BiP* or *CHOP* on SH-SY5Y cells after tunicamycin. *BiP* and *CHOP* mRNA levels were measured using a quantitative real-time PCR.
(TIF)

Figure S4 SUN N8075 protect cell death induced by tunicamycin, but did not affect protein expression of ATF4, BiP or CHOP in RGC-5 cells. (*A*) SUN N8075 at 0.1 to 3 μM shows protective effect on the reduction of cell viability at 24 h after tunicamycin at 2 μg/ml. Each column represents the mean ± S.E.M. (n = 8). ##p<0.01 versus control. **p<0.01 versus tunicamycin alone. (*B*) ATF4, BiP and CHOP protein levels were measured using Western blotting.
(TIF)

Figure S5 SUN N8075 enhances survival signals via Akt and ERK1/2 activations. (*A*) Time-course of changes in phosphorylated-Akt level after SUN N8075 treatment. (*B*) Concentration-dependent changes in phosphorylated-Akt level at 24 h after SUN N8075 treatment. (*C, D*) Tunicamycin reduced phosphorylated-Akt (*C*) and phosphorylated-ERK1/2 (*D*) levels, and their reductions were ameliorated by SUN N8075 treatment. (*E, F*) The protective effect of SUN N8075 on tunicamycin-induced reduction of cell viability was eliminated by LY294002, a PI3kinase inhibitor, at 20 μM (*E*) or U0126, a MEK1/2 inhibitor, at 5 μM (*F*).
(TIF)

Figure S6 Effects of SUN N8075 on body weight changes in two type of familial ALS model animals. (*A*) Effect of SUN N8075 at 30 mg/kg/day, s.c. on body weight change in G93A mutant SOD1 mice. (*B*) Effect of SUN N8075 at 10 mg/kg/day, s.c. on body weight change in H46R mutant SOD1 rats.
(TIF)

Figure S7 (*A*) Volcano plot of probe data set averages of gene expressions in the spinal cords of G93A (n = 4) compared with WT (n = 4). The x-axis and y-axis correspond to the average fold-change (FC), and the negative log10-transformed p value between G93A and WT mice, respectively. Green (FC ≥2, 0.01≤p≤0.05) and red (FC ≥2, p≤0.01) squares represent significantly differentially expressed probe sets, and gray squares represent probe sets with no significant difference between G93A and WT mice. The changes in gene expression were considered statistically significant based on the criteria of FC ≥2, p≤0.01 with Benjamini-Hochberg correction. (*B*) Heat map representation of hierarchical clustering of 712 different gene expressions in the spinal cords of G93A compared with WT mice. The columns and rows represent the tissue samples (WT = Blue, G93A = red, G93A + SUN N8075 = yellow) and individual gene expressions, respectively. Shades of red indicate elevated expression while shades of blue indicate decreased expression relative to the median (see the color scale). (*C*) Principal components analysis (PCA) in the spinal cord of WT, G93A and G93A + SUN N8075 treated mice. Differently expressed 712 genes in the two groups (WT vs. G93A mice) were analyzed using a principal component analysis, and the

contribution rates of genes to PCA component 1, 2, and 3 were 81.23%, 6.99%, and 3.90%, respectively. The results are expressed as a one-dimensional function with PCA component 1 that defines the direction of greatest variation in the probe/gene transcriptomic feature space. ##$p<0.01$, *$p<0.05$, Student's t-test. (*D*) Gene ontology classification for each category from the 712 different genes.
(TIF)

Table S1 Clinical information about the spinal cord tissues from patients with sporadic ALS (a) and for control (b). M, male; F, female; PMI, post mortem interval; y, years; m, months; h, hours.
(PDF)

Table S2 Gene expression profiles after SUN N8075 treatment in SH-SY5Y cells.
(PDF)

Table S3 Gene expression profiles for ER-stress responsible genes after SUN N8075 alone, or tunicamycin with or without SUN N8075 in SH-SY5Y cells. ↑: two-fold or more increase, →: no changes.
(PDF)

Table S4 SUN N8075 prolongs disease onset and lifspan in a rat model of familial ALS. Data are the means ± S.E. (n = 9 or 10), * $P<0.05$ vs vehicle-treated ALS mouse group. a Observable functional deficits (motor score of 4), b Righting reflex failure (motor score of 1), c Motor score of 0.
(PDF)

Acknowledgments

We thank Professor Takashi Inuzuka and Professor Isao Hozumi, Department of Neurology and Geriatrics, Gifu University of Medicine, Japan for critical discussions and advice, and Dr. Neeraj Agarwal, Department of Pathology and Anatomy, University of Texas Health Science Center (Fort Worth, TX), for the kind gift of RGC-5.

Author Contributions

Conceived and designed the experiments: MS HH. Performed the experiments: HT YI NM KT MY. Analyzed the data: MS HT YI KT MK ST. Contributed reagents/materials/analysis tools: TI HT HW MA. Wrote the paper: MS HH.

References

1. Kaufman RJ (1999) Stress signaling from the lumen of the endoplasmic reticulum: coordination of gene transcriptional and translational controls. Genes Dev 13: 1211–1233.
2. Yoshida H (2007) ER stress and diseases. FEBS J 274: 630–658.
3. Harding HP, Calfon M, Urano F, Novoa I, Ron D (2002) Transcriptional and translational control in the Mammalian unfolded protein response. Annu Rev Cell Dev Biol 18: 575–599.
4. Atkin JD, Farg MA, Turner BJ, Tomas D, Lysaght JA, et al. (2006) Induction of the unfolded protein response in familial amyotrophic lateral sclerosis and association of protein-disulfide isomerase with superoxide dismutase 1. J Biol Chem 281: 30152–30165.
5. Atkin JD, Farg MA, Walker AK, McLean C, Tomas D, et al. (2008) Endoplasmic reticulum stress and induction of the unfolded protein response in human sporadic amyotrophic lateral sclerosis. Neurobiol Dis 30: 400–407.
6. Ilieva EV, Ayala V, Jove M, Dalfo E, Cacabelos D, et al. (2007) Oxidative and endoplasmic reticulum stress interplay in sporadic amyotrophic lateral sclerosis. Brain 130: 3111–3123.
7. Nagata T, Ilieva H, Murakami T, Shiote M, Narai H, et al. (2007) Increased ER stress during motor neuron degeneration in a transgenic mouse model of amyotrophic lateral sclerosis. Neurol Res 29: 767–771.
8. Wootz H, Hansson I, Korhonen L, Napankangas U, Lindholm D (2004) Caspase-12 cleavage and increased oxidative stress during motoneuron degeneration in transgenic mouse model of ALS. Biochem Biophys Res Commun 322: 281–286.
9. Annoura H, Nakanishi K, Toba T, Takemoto N, Imajo S, et al. (2000) Discovery of (2S)-1-(4-amino-2,3,5- trimethylphenoxy)-3-[4-[4-(4- fluorobenzyl)-phenyl]-1-piperazinyl]-2-propanol dimethanesulfonate (SUN N8075): a dual Na^+ and Ca^{2+} channel blocker with antioxidant activity. J Med Chem 43: 3372–3376.
10. Possenti R, Eldridge JD, Paterson BM, Grasso A, Levi A (1989) A protein induced by NGF in PC12 cells is stored in secretory vesicles and released through the regulated pathway. EMBO J 8: 2217–2223.
11. Alder J, Thakker-Varia S, Bangasser DA, Kuroiwa M, Plummer MR, et al. (2003) Brain-derived neurotrophic factor-induced gene expression reveals novel actions of VGF in hippocampal synaptic plasticity. J Neurosci 23: 10800–10808.
12. Salton SR, Ferri GL, Hahm S, Snyder SE, Wilson AJ, et al. (2000) VGF: a novel role for this neuronal and neuroendocrine polypeptide in the regulation of energy balance. Front Neuroendocrinol 21: 199–219.
13. Zhao Z, Lange DJ, Ho L, Bonini S, Shao B, et al. (2008) Vgf is a novel biomarker associated with muscle weakness in amyotrophic lateral sclerosis (ALS), with a potential role in disease pathogenesis. Int J Med Sci 5: 92–99.
14. Maruyama W, Akao Y, Carrillo MC, Kitani K, Youdim MB, et al. (2002) Neuroprotection by propargylamines in Parkinson's disease: suppression of apoptosis and induction of prosurvival genes. Neurotoxicol Teratol 24: 675–682.
15. Jiang Y, Ahn EY, Ryu SH, Kim DK, Park JS, et al. (2004) Cytotoxicity of psammaplin A from a two-sponge association may correlate with the inhibition of DNA replication. BMC Cancer 4: 70.
16. Gurney ME (1997) The use of transgenic mouse models of amyotrophic lateral sclerosis in preclinical drug studies. J Neurol Sci 152(Suppl 1): S67–73.
17. Nagai M, Aoki M, Miyoshi I, Kato M, Pasinelli P, et al. (2001) Rats expressing human cytosolic copper-zinc superoxide dismutase transgenes with amyotrophic lateral sclerosis: associated mutations develop motor neuron disease. J Neurosci 21: 9246–9254.
18. Sun W, Funakoshi H, Nakamura T (2002) Overexpression of HGF retards disease progression and prolongs life span in a transgenic mouse model of ALS. J Neurosci 22: 6537–6548.
19. Chiba T, Yamada M, Sasabe J, Terashita K, Aiso S, et al. (2006) Colivelin prolongs survival of an ALS model mouse. Biochem Biophys Res Commun 343: 793–798.
20. Matsumoto A, Okada Y, Nakamichi M, Nakamura M, Toyama Y, et al. (2006) Disease progression of human SOD1 (G93A) transgenic ALS model rats. J Neurosci Res 83: 119–133.
21. Hitomi J, Katayama T, Taniguchi M, Honda A, Imaizumi K, et al. (2004) Apoptosis induced by endoplasmic reticulum stress depends on activation of caspase-3 via caspase-12. Neurosci Lett 357: 127–130.
22. Kleizen B, Braakman I (2004) Protein folding and quality control in the endoplasmic reticulum. Curr Opin Cell Biol 16: 343–349.
23. Gething MJ (1999) Role and regulation of the ER chaperone BiP. Semin Cell Dev Biol 10: 465–472.
24. Oyadomari S, Mori M (2004) Roles of CHOP/GADD153 in endoplasmic reticulum stress. Cell Death Differ 11: 381–389.
25. Hawley RJ, Scheibe RJ, Wagner JA (1992) NGF induces the expression of the VGF gene through a cAMP response element. J Neurosci 12: 2573–2581.
26. Bozdagi O, Rich E, Tronel S, Sadahiro M, Patterson K, et al. (2008) The neurotrophin-inducible gene Vgf regulates hippocampal function and behavior through a brain-derived neurotrophic factor-dependent mechanism. J Neurosci 28: 9857–9869.
27. Thakker-Varia S, Krol JJ, Nettleton J, Bilimoria PM, Bangasser DA, et al. (2007) The neuropeptide VGF produces antidepressant-like behavioral effects and enhances proliferation in the hippocampus. J Neurosci 27: 12156–12167.
28. Almeida RD, Manadas BJ, Melo CV, Gomes JR, Mendes CS, et al. (2005) Neuroprotection by BDNF against glutamate-induced apoptotic cell death is mediated by ERK and PI3-kinase pathways. Cell Death Differ 12: 1329–1343.
29. Hu P, Han Z, Couvillon AD, Exton JH (2004) Critical role of endogenous Akt/IAPs and MEK1/ERK pathways in counteracting endoplasmic reticulum stress-induced cell death. J Biol Chem 279: 49420–49429.
30. Sasaki S, Nagai M, Aoki M, Komori T, Itoyama Y, et al. (2007) Motor neuron disease in transgenic mice with an H46R mutant SOD1 gene. J Neuropathol Exp Neurol 66: 517–524.
31. Pasinetti GM, Ungar LH, Lange DJ, Yemul S, Deng H, et al. (2006) Identification of potential CSF biomarkers in ALS. Neurology 66: 1218–1222.
32. Levi A, Ferri GL, Watson E, Possenti R, Salton SR (2004) Processing, distribution, and function of VGF, a neuronal and endocrine peptide precursor. Cell Mol Neurobiol 24: 517–533.
33. Liu JW, Andrews PC, Mershon JL, Yan C, Allen DL, et al. (1994) Peptide V: a VGF-derived neuropeptide purified from bovine posterior pituitary. Endocrinology 135: 2742–2748.
34. Trani E, Giorgi A, Canu N, Amadoro G, Rinaldi AM, et al. (2002) Isolation and characterization of VGF peptides in rat brain. Role of PC1/3 and PC2 in the maturation of VGF precursor. J Neurochem 81: 565–574.

35. Ruetschi U, Zetterberg H, Podust VN, Gottfries J, Li S, et al. (2005) Identification of CSF biomarkers for frontotemporal dementia using SELDI-TOF. Exp Neurol 196: 273–281.
36. Succu S, Mascia MS, Melis T, Sanna F, Melis MR, et al. (2005) Pro-VGF-derived peptides induce penile erection in male rats: Involvement of paraventricular nitric oxide. Neuropharmacology 49: 1017–1025.
37. Hunsberger JG, Newton SS, Bennett AH, Duman CH, Russell DS, et al. (2007) Antidepressant actions of the exercise-regulated gene VGF. Nat Med 13: 1476–1482.
38. Bartolomucci A, La Corte G, Possenti R, Locatelli V, Rigamonti AE, et al. (2006) TLQP-21, a VGF-derived peptide, increases energy expenditure and prevents the early phase of diet-induced obesity. Proc Natl Acad Sci U S A 103: 14584–14589.
39. Severini C, Ciotti MT, Biondini L, Quaresima S, Rinaldi AM, et al. (2008) TLQP-21, a neuroendocrine VGF-derived peptide, prevents cerebellar granule cells death induced by serum and potassium deprivation. J Neurochem 104: 534–544.
40. Goodall EF, Morrison KE (2006) Amyotrophic lateral sclerosis (motor neuron disease): proposed mechanisms and pathways to treatment. Expert Rev Mol Med 8: 1–22.
41. Pioro EP, Mitsumoto H (1995) Animal models of ALS. Clin Neurosci 3: 375–385.

Journal of Neuroscience Research

Journal of Neuroscience Research 88:2736–2746 (2010)

Appearance of Phagocytic Microglia Adjacent to Motoneurons in Spinal Cord Tissue From a Presymptomatic Transgenic Rat Model of Amyotrophic Lateral Sclerosis

Tomomi Sanagi,[1] Shigeki Yuasa,[2] Yasuko Nakamura,[1] Eri Suzuki,[1] Masashi Aoki,[3] Hitoshi Warita,[3] Yasuto Itoyama,[3] Shigeo Uchino,[1] Shinichi Kohsaka,[1]* and Keiko Ohsawa[1]

[1]Department of Neurochemistry, National Institute of Neuroscience, Kodaira, Japan
[2]Department of Ultrastructural Research, National Institute of Neuroscience, Kodaira, Japan
[3]Department of Neurology, Tohoku University School of Medicine, Sendai, Japan

Microglial activation occurs early during the pathogenesis of amyotrophic lateral sclerosis (ALS). Recent evidence indicates that the expression of mutant Cu^{2+}/Zn^{2+} superoxide dismutase 1 (SOD1) in microglia contributes to the late disease progression of ALS. However, the mechanism by which microglia influence the neurodegenerative process and disease progression in ALS remains unclear. In this study, we revealed that activated microglia aggregated in the lumbar spinal cord of presymptomatic mutant $SOD1^{H46R}$ transgenic rats, an animal model of familial ALS. The aggregated microglia expressed a marker of proliferating cell, Ki67, and phagocytic marker proteins ED1 and major histocompatibility complex (MHC) class II. The motoneurons near the microglial aggregates showed weak choline acetyltransferase (ChAT) immunoreactivity and contained reduced granular endoplasmic reticulum and altered nucleus electron microscopically. Furthermore, immunopositive signals for tumor necrosis factor-α (TNFα) and monocyte chemoattractant protein-1 (MCP-1) were localized in the aggregated microglia. These results suggest that the activated and aggregated microglia represent phagocytic features in response to early changes in motoneurons and possibly play an important role in ALS disease progression during the presymptomatic stage.

Key words: microglia; phagocytosis; mutant SOD1; immunohistochemistry; electron microscopy

Amyotrophic lateral sclerosis (ALS) is an adult-onset neurodegenerative disease that selectively affects motoneurons in the brain and spinal cord. It is characterized by progressive muscle weakness, amyotrophy, and death from respiratory paralysis, usually within 3–5 years of onset (Bruijn et al., 2004; Boillee et al., 2006a). Dominant mutations in the gene encoding the ubiquitously expressed Cu^{2+}/Zn^{2+} superoxide dismutase 1 (SOD1) are the most prominent known causes of familial ALS (Aoki et al., 1993; Rosen, 1993; Rosen et al., 1994). Transgenic animals overexpressing the mutant form of human SOD1 develop a progressive motoneuron disease with many clinical and pathological features similar to those observed in ALS patients (Aoki et al., 2005). Mutant SOD1 has been reported to induce selective motoneuron loss through a combination of several mechanisms, including protein aggregation, mitochondrial dysfunction, oxidative stress, excitotoxicity, and inflammation (Mattiazzi et al., 2002; Bruijn et al., 2004; Boillee et al., 2006a; Saxena et al., 2009).

Accumulating evidence suggests that glial cells are involved in ALS pathogenesis (Neusch et al., 2007). Abundant glial activation has been described in the brain and spinal cord, both in human ALS patients and in various mutant SOD1 transgenic mouse models (Hall et al., 1998b; Anneser et al., 2004; Neusch et al., 2007). Mutant SOD1 expression in neurons alone was not sufficient to cause motoneuron loss and motor deficits in mutant SOD1 transgenic mice (Pramatarova et al., 2001; Lino et al., 2002). A study using chimeric mice with

Additional Supporting Information may be found in the online version of this article.

Contract grant sponsor: Japanese Ministry of Health, Labour and Welfare; Contract grant sponsor: Japanese Ministry of Education, Culture, Sports, Science and Technology; Contract grant number: 21500363.

*Correspondence to: Dr. Shinichi Kohsaka, Department of Neurochemistry, National Institute of Neuroscience, 4-1-1 Ogawahigashi, Kodaira, Tokyo 187-8502, Japan. E-mail: kohsaka@ncnp.go.jp

Received 19 December 2009; Revised 17 February 2010; Accepted 1 April 2010

Published online 27 May 2010 in Wiley InterScience (www.interscience.wiley.com). DOI: 10.1002/jnr.22424

mixtures of wild-type and mutant SOD1-expressing cells showed that mutant SOD1-expressing nonneuronal cells induced mutant SOD1-negative motoneuron death, whereas mutant SOD1-negative nonneuronal cells extended mutant SOD1-expressing motoneuron survival (Clement et al., 2003). These results indicate that the presence of nonneuronal cells expressing mutant SOD1 near motoneurons contributes to motoneuron death.

Microglia are the main inflammatory cells of the central nervous system (CNS) and play an important role in the immunoregulation by interacting with neurons, astrocytes, and other glial cells. Activated microglia are observed in various neurodegenerative diseases and produce both inflammatory mediators and neuroprotective factors (Nakajima and Kohsaka, 2001, 2004). Recent studies have reported that diminishing mutant SOD1 levels in microglia slow disease progression in mutant $SOD1^{G93A}$ mice during the later stage (Boillee et al., 2006b) and that wild-type donor-derived microglia promote neuroprotection and extend survival in mutant $SOD1^{G93A}$/PU.1 knockout mice (Beers et al., 2006). In mutant SOD1-mediated ALS model mice, activated microglia are observed in the lumbar spinal cord before disease onset, and the number of activated cells increases during disease progression (Hall et al., 1998b; Alexianu et al., 2001). Indeed, inflammatory-related cytokines and chemokines are reportedly elevated in the cerebrospinal fluid and CNS tissues of ALS patients and ALS animal models (Sargsyan et al., 2005). These results suggest that microglia might contribute to the propagation of the disease process in ALS. However, the exact contribution of microglia to the neurodegenerative process in ALS remains unclear. Therefore, in this study, we used immunohistochemistry and electron microscopy to examine the function of activated microglia in the spinal cord of mutant $SOD1^{H46R}$ rats during the presymptomatic stage.

MATERIALS AND METHODS

Animal Subjects

All the animal experiments were performed according to the guidelines for the care and use of laboratory animals approved by the National Institute of Neuroscience. Rat transgenic for the H46R-mutated human SOD1 (mutant $SOD1^{H46R}$ rats) were provided by Dr. Masashi Aoki (Tohoku University School of Medicine, Sendai, Japan). Transgenic rats were maintained as hemizygotes by mating transgenic males with wild-type Sprague-Dawley females and were identified by using polymerase chain reaction (PCR). The time of disease onset was identified by the onset of weight loss, reflecting denervation-induced muscle atrophy as previously described (Nagai et al., 2001). In the present study, the presymptomatic stage (150 days of age) was defined as the time at which the rats reached their peak body weight (Supp. Info. Fig. 1A). The body weight of mutant $SOD1^{H46R}$ rats at the presymptomatic stage was almost the same as that of wild-type rats (149.8 days of age). The early disease stage (180.5 days of age) was defined as the time at which the rats had experienced a 10% weight loss, and the end stage (196.5 days of age) was defined as the time at which the rats had experienced a 30% weight loss (Supp. Info. Fig. 1A).

Perfusion and Tissue Processing

Rats were deeply anesthetized with ether and then perfused transcardially with PBS, followed by 4% paraformaldehyde in PBS. The fixed spinal cord was removed and stored in 4% paraformaldehyde at 4°C for 24 hr. The lumbar spinal cord (L4–L5 region) was cryoprotected for 48 hr in 30% sucrose in PBS and embedded in OCT medium (Sakura Finetek Japan, Tokyo, Japan). Embedded tissue was quickly frozen with dry ice and stored at −80°C until the preparation of 20-μm sections on a cryostat (CM-3000; Leica, Wetzlar, Germany), which were subsequently subjected to immunohistochemical analysis.

Nissl Staining and Motoneuron Cell Counting

Every thirtieth spinal cord section (580-μm interval) was stained with 0.1% cresyl violet acetate (Wako, Osaka, Japan) for 30 min at room temperature. After three washes with PBS, the sections were dehydrated by passing through 70%, 80%, 90%, and 100% ethanol, followed by xylene, then coverslipped (Entellan New; Merck, Darmstadt, Germany). The tissues were examined via light microscopy (ME600; Nikon, Tokyo, Japan), and the number of motoneurons with nuclei located in the anterior horn was counted in four sections. The number of Nissl-stained motoneurons was expressed as a percentage of the number observed in wild-type rats.

Immunohistochemical Staining

Tissue sections were permeabilized with PBS containing 0.3% Triton X-100 (PBST) at room temperature for 30 min. After three washes with PBS, background staining was blocked by incubating for 2 hr in 1% bovine serum albumin (BSA; Sigma, St. Louis, MO) containing 0.3% Triton X-100 (1% BSA in PBST), followed by incubation with the following primary antibodies in 1% BSA in PBST at 4°C overnight: rabbit anti-ionized calcium binding adaptor molecule 1 (Iba1; diluted 1:1,000; Imai et al., 1996), goat anti-choline acetyltransferase (ChAT; diluted 1:200; Millipore, Temecula, CA), mouse anti-OX-42 (diluted 1:200; Millipore), mouse anti-Ki67 (diluted 1:100; Novocastra, Newcastle, United Kingdom), mouse anti-ED1 (diluted 1:500; Serotec, Oxford, United Kingdom), mouse anti-major histocompatibility complex (MHC) class II (diluted 1:400; Abcam, Tokyo, Japan), goat anti-tumor necrosis factor-α (TNFα; 5 μg/ml; R&D Systems, Minneapolis, MN), and goat anti-monocyte chemoattractant protein-1 (MCP-1; diluted 1:50; Santa Cruz Biotechnology, Santa Cruz, CA). The sections were then washed extensively with PBS and subjected to further incubation for 2 hr with the following secondary antibodies in 1% BSA in PBST at 4°C: Alexa Fluor 488-conjugated anti-goat or mouse IgG (diluted 1:1,000; Invitrogen, Carlsbad, CA) or Cy3-conjugated anti-rabbit IgG (diluted 1:200; Jackson Immunoresearch, West Grove, PA). For fluorescent Nissl staining, the sections were incubated with green fluorescent Nissl stain (Invitrogen) at a dilution of 1:300 for 1 hr and then counter-

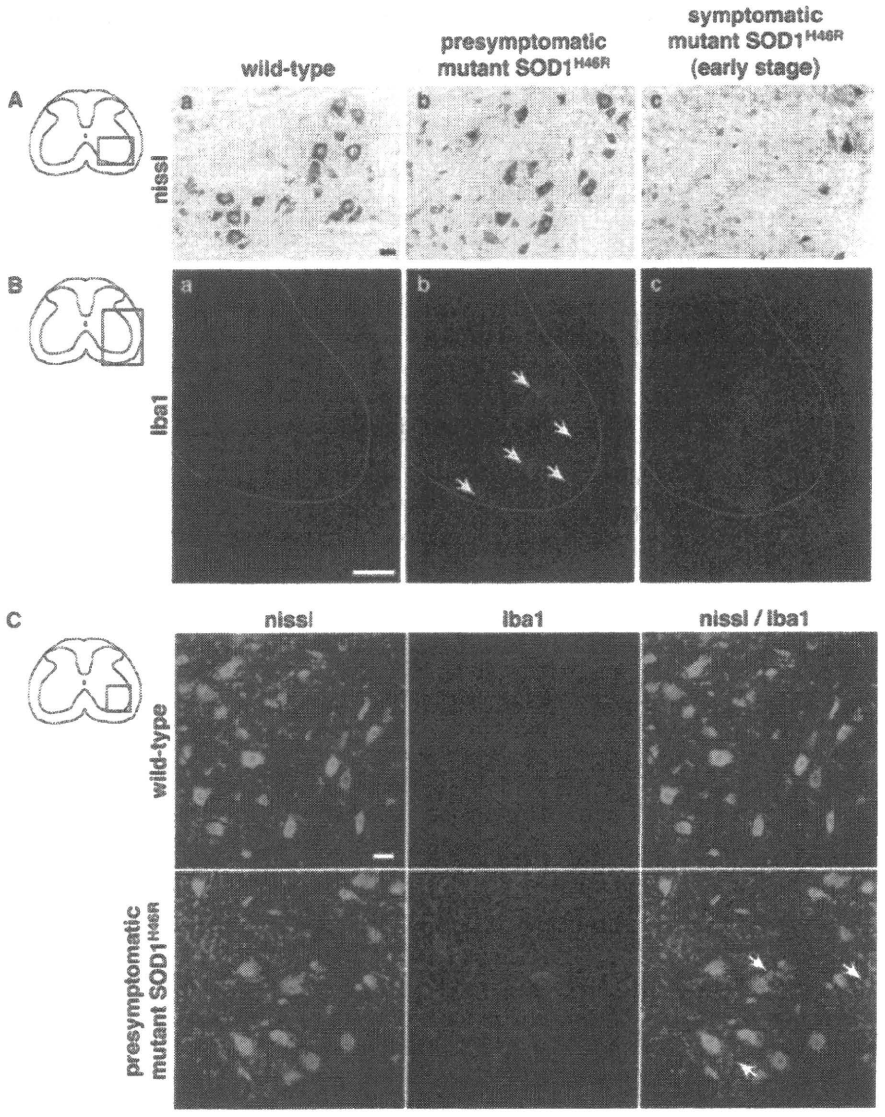

Fig. 1. **A**: Photomicrographs showing Nissl-stained lumbar spinal cord sections of wild-type (a), presymptomatic mutant $SOD1^{H46R}$ (b), and symptomatic (early-stage) mutant $SOD1^{H46R}$ (c) rats. **B**: Spinal cord sections of wild-type (a), presymptomatic mutant $SOD1^{H46R}$ (b), and symptomatic (early-stage) mutant $SOD1^{H46R}$ (c) rats were immunostained with anti-Iba1 antibody. Iba1-positive microglial aggregates (arrows) were observed in the anterior horn of presymptomatic mutant $SOD1^{H46R}$ rats (b). Iba1 immunoreactivity was significantly increased in the anterior horn of symptomatic mutant $SOD1^{H46R}$ rats (c). Dotted lines indicate the border between the white matter and the gray matter. **C**: Nissl staining (green) and Iba1 immunostaining (red) in the anterior horn of wild-type and presymptomatic mutant $SOD1^{H46R}$ rats. Activated microglia have aggregated around the motoneurons. Arrows indicate the microglial aggregates. Scale bars = 50 μm in A,C; 0.3 mm in B.

stained with 1 μg/ml 4′,6-diamidino-2-phenylindole (DAPI; Dojindo, Kumamoto, Japan) to visualize the nuclei. After three washes, the sections were coverslipped (Fluoromount; Diagnostic BioSystems, Pleasanton, CA). The images shown in Figure 1B were collected with a fluorescent microscope (AX70; Olympus, Tokyo, Japan). The images shown in Figures 1C, 2, and 3 were collected with a confocal laser microscope (FV1000; Olympus), and 10 XY images acquired at 1-μm z-step intervals were merged. In Figure 5, a 1-μm-thick XY image as observed through a confocal laser microscope is shown.

Electron Microscopy

Rats were deeply anesthetized by intraperitoneal injection of pentobarbital (50 mg/kg) and were perfusion fixed transcardially with 2% paraformaldehyde and 2.5% glutaraldehyde in

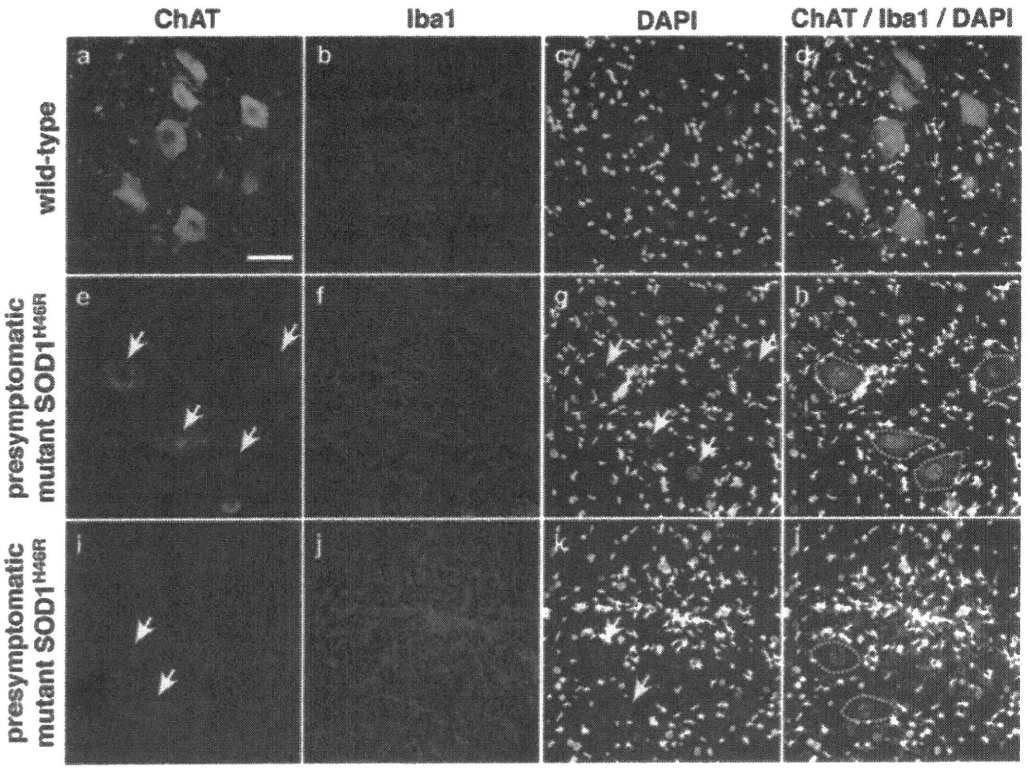

Fig. 2. **a–l**: Spinal cord sections of wild-type and presymptomatic mutant $SOD1^{H46R}$ rats were immunostained with anti-ChAT (green) and anti-Iba1 (red) antibodies and were counterstained with DAPI (white). Arrows in e and i indicate the weak expression of ChAT in motoneurons. Arrows in g and k indicate the nuclei of the motoneurons, which were weakly immunoreactive for ChAT. ChAT immunoreactivity (green) was decreased in the motoneurons in the anterior horn of presymptomatic mutant $SOD1^{H46R}$ rats compared with wild-type rats. In particular, the motoneurons near the microglial aggregates were weakly immunoreactive for ChAT despite their well-preserved nuclei. Scale bar = 50 μm.

PBS. The fixed spinal cord was removed, and the excised lumbar enlargement was embedded in 3% agarose in PBS. Transverse sections (70 μm thickness) were prepared by using a Microslicer (DTK-3000; Dosaka EM, Kyoto, Japan), and the sections of L4–L5 region were selected under microscopic observation. The selected sections were rinsed, osmicated, dehydrated, and embedded in epoxy resin. First, the anterior horn was excised, and sections of 1-μm thickness (semithin sections) were prepared. Semithin sections were stained with toluidine blue for light microscopic observation, and finally the lamina VIII–IX were selected. Then, ultrathin sections of the lamina were prepared, stained with lead citrate and uranyl acetate, and observed under a Hitachi H-7000 transmission electron microscope (Hitachi High-Tech, Tokyo, Japan). Microglia were morphologically identified based on the description in *The fine structure of the nervous system* (Peters et al., 1991).

RESULTS

Aggregated Microglia in the Lumbar Spinal Cord of Presymptomatic Mutant $SOD1^{H46R}$ Rats

To understand the activation pattern of the microglia during the disease process in mutant $SOD1^{H46R}$ rats, we examined Iba1 immunoreactivity in the lumbar spinal cord tissues of wild-type, presymptomatic mutant $SOD1^{H46R}$, and symptomatic mutant $SOD1^{H46R}$ rats. The survival of motoneurons at the presymptomatic and symptomatic stage was evaluated by counting the number of Nissl-stained motoneurons in the anterior horn of the lumbar spinal cord of wild-type and mutant $SOD1^{H46R}$ rats. Overall, 98.5% ± 2.2% of the Nissl-stained motoneurons were preserved in the gray matter of the lumbar spinal cord sections of presymptomatic mutant $SOD1^{H46R}$ rats, whereas the number of Nissl-stained motoneurons in early symptomatic mutant $SOD1^{H46R}$ rats decreased to 21.89% ± 0% of the total motoneurons in wild-type rats (Fig. 1A, Supp. Info. Fig. 1B). In wild-type rats, the microglia exhibited a small cell body with highly ramified processes and were distributed throughout the lumbar spinal cord (Fig. 1Ba). Iba1 immunoreactivity was increased in the anterior horn of mutant $SOD1^{H46R}$ rats at the presymptomatic stage (Fig. 1Bb) and was further increased at the symptomatic stage (Fig. 1Bc). In presymptomatic mutant $SOD1^{H46R}$ rats, the microglia formed aggregates in the anterior horn of the lum-

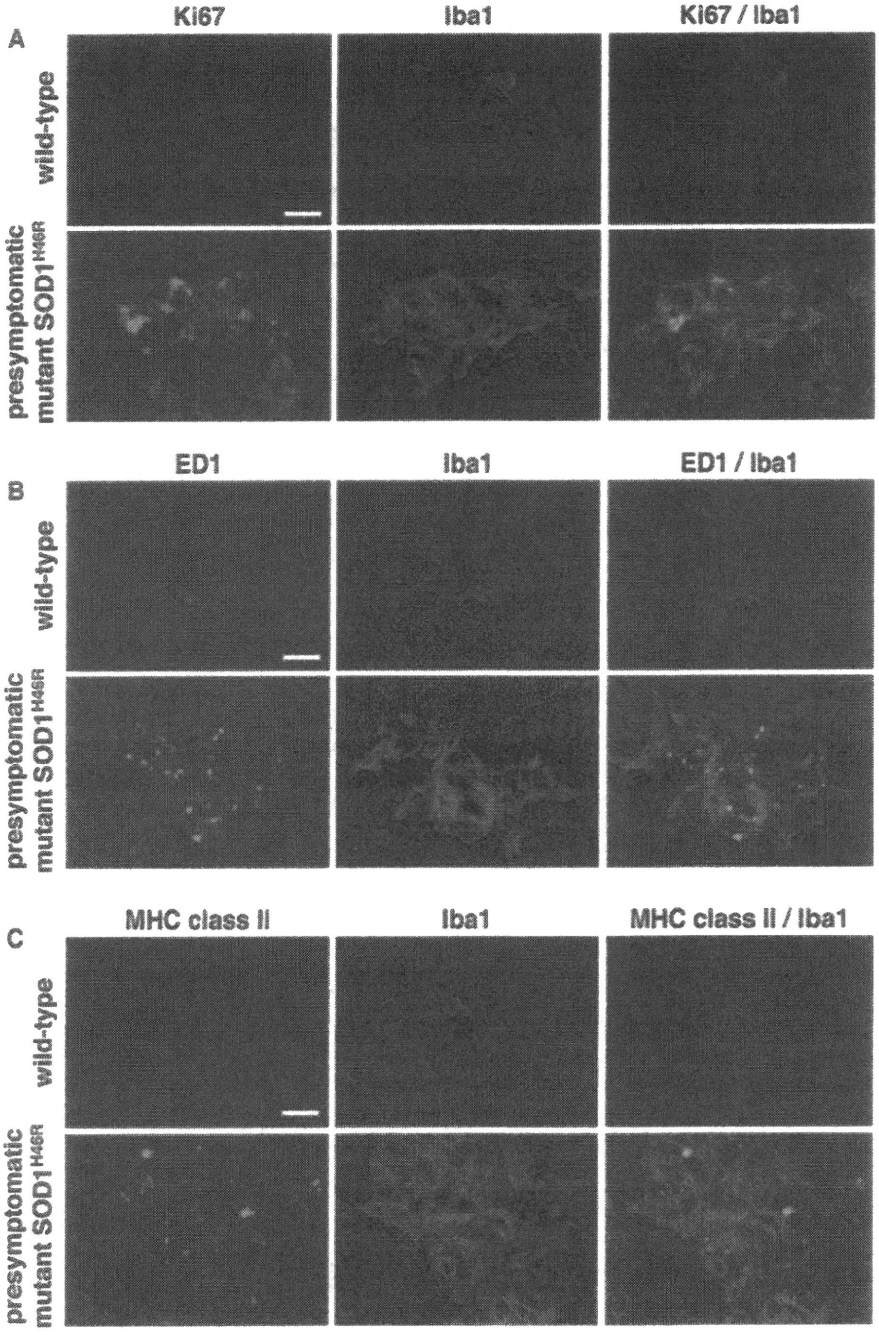

Fig. 3. Spinal cord sections of wild-type and presymptomatic mutant $SOD1^{H46R}$ rats were immunostained with anti-Ki67 (green in A), anti-ED1 (green in B), anti-MHC class II (green in C), and anti-Iba1 (red) antibodies. **A**: Microglial aggregates observed in the anterior horn of presymptomatic mutant $SOD1^{H46R}$ rats were immunoreactive for Ki67. **B,C**: Iba1-positive microglial aggregates were immunoreactive for ED1 (B) and MHC class II (C). Scale bars = 10 μm.

bar spinal cord (arrows in Fig. 1Bb). To examine the location of the aggregated microglia in the anterior horn, we performed Nissl staining and Iba1 immunostaining. Aggregated microglia were found around Nissl-stained motoneurons in the anterior horn of the lumbar spinal cord (Fig. 1C).

ChAT Immunoreactivity in Motoneurons of the Lumbar Spinal Cord

To determine whether the motoneurons in presymptomatic mutant $SOD1^{H46R}$ rats had undergone functional changes, compared with healthy motoneurons in wild-type rats, we examined ChAT immunoreactivity in the motoneurons of the lumbar spinal cord. ChAT is a marker molecule that reflects the functional activity of motoneurons. ChAT immunoreactivity was obviously decreased in the motoneurons of the lumbar spinal cord of presymptomatic mutant $SOD1^{H46R}$ rats compared with wild-type rats (Fig. 2e, Supp. Info. Fig. 1C). In particular, ChAT immunoreactivity in the motoneurons near aggregated microglia was barely detectable (Fig. 2i).

Characterization of Aggregated Microglia

The microglial aggregates observed in the lumbar spinal cord of presymptomatic mutant $SOD1^{H46R}$ rats comprised clusters of numerous microglia (Supp. Info. Fig. 2A). To determine whether the aggregated microglia were proliferative, we immunostained the aggregated microglia using an antibody against Ki67, a marker of proliferating cells. Some microglia in the aggregate were immunopositive for Ki67 (Fig. 3A).

When the brain is injured, the resident ramified microglia transform into activated microglia, and the expression of the microglial marker OX-42 increases. In the lumbar spinal cord sections, the expression of OX-42 was elevated in the microglia of presymptomatic mutant $SOD1^{H46R}$ rats compared with wild-type rats (Supp. Info. Fig. 2B), and strong immunoreactivity for OX-42 was observed in the aggregated microglia (arrows in Supp. Info. Fig. 2B). Activated microglia are known to phagocyte neural and myelin debris. Therefore, immunohistochemistry for ED1 and MHC class II, which are phagocytic marker proteins, was performed to determine whether the aggregated microglia were phagocytic. Immunopositive signals for ED1 and MHC class II were localized in the aggregated microglia observed in the lumbar spinal cords of presymptomatic mutant $SOD1^{H46R}$ rats (Fig. 3B,C).

Ultrastructure of the Microglia and Neuronal Component in the Anterior Horn

As observed microscopically in the toluidine blue-stained sections, few glial cells were attached to the somata of motoneurons in the anterior horn of the lumbar spinal cord of the wild-type rat (Supp. Info. Fig. 3Aa). In the mutant $SOD1^{H46R}$ rat, glial cells increased in the anterior horn and were attached to the somata of motoneurons as early as the presymptomatic stage (Supp. Info. Fig. 3Ab), and significantly increased glial cells surrounded the somata of motoneurons exhibiting reduced Nissl bodies and altered nucleus at the early symptomatic stage (Supp. Info. Fig. 3Ac).

Ultrastructural characteristics to identify microglia are as follows: the nucleus is oval or elongated, with prominent chromatin clumps beneath the nuclear envelope and throughout the nucleoplasm. The cytoplasm extends out in broad processes invading the surrounding neuropil. Droplets, lysosomes, lipofuscin, and ingested material are present in the cytoplasm. Electron microscopically, granular endoplasmic reticulum was abundant in the perikarya of the motoneurons (Fig. 4A), and clusters of ribosomes were arranged between the flattened cisternae (Supp. Info. Fig. 3Ba) in the anterior horn of the wild-type rat. Isolated microglia were occasionally found around the somata of motoneurons without direct attachment (Supp. Info. Fig. 3Bb). In the anterior horn of the mutant $SOD1^{H46R}$ rat, microglia surrounded the motoneurons (Fig. 4B,C) and directly attached to the somata (Supp. Info. Fig. 3Bc) as early as the presymptomatic stage. Microglia exhibited various patterns of distribution; several isolated microglia were attached to the somata of motoneurons that contained the granular endoplasmic reticulum abundantly and exhibited the appearance of normal morphology (Fig. 4B), and the somata of motoneurons with reduced granular endoplasmic reticulum and altered nucleus were surrounded by clusters of microglia (Fig. 4C). Large clusters of microglia with many processes were found among the motoneurons and surrounded the neuropils (Fig. 4D). These microglia represented typical morphology; the oval to elongated nucleus has large clumps of chromatin beneath the nuclear envelope, and many inclusion bodies, dark lipofuscin granules, degenerating axons and long cisternae of the granular endoplasmic reticulum were contained in the dark cytoplasm (Fig. 4E). At the early symptomatic stage, the numbers of microglia with many processes significantly increased and extensively surrounded the somata and neuritis of still surviving motoneurons (Supp. Info. Fig. 3Bd).

Immunoreactivity for TNFα and MCP-1 in Aggregated Microglia

In the CNS tissues of mutant SOD1 transgenic mice, the expression of TNFα and MCP-1 has been shown to be elevated (Henkel et al., 2004; Cereda et al., 2008; Liu et al., 2009). Next, we immunostained the lumbar spinal cord sections of wild-type and presymptomatic mutant $SOD1^{H46R}$ rats with anti-TNFα and MCP-1 antibodies. Ramified microglia were immunonegative for TNFα and MCP-1 in the anterior horn of wild-type rats (Fig. 5Ab,Bb). Immunopositive signals for TNFα and MCP-1 were increased in the anterior horn of presymptomatic mutant $SOD1^{H46R}$ rats compared with wild-type rats (Fig. 5Ac,Bc), and the aggregated microglia were immunoreactive for TNFα and MCP-1 (Fig. 5Ad,Bd).

DISCUSSION

In this study, we revealed that activated microglia aggregate near motoneurons in the lumbar spinal cord of mutant $SOD1^{H46R}$ transgenic rats during the presymptomatic stage. The number of Nissl-stained motoneurons was not decreased in the lumbar spinal cords of pre-

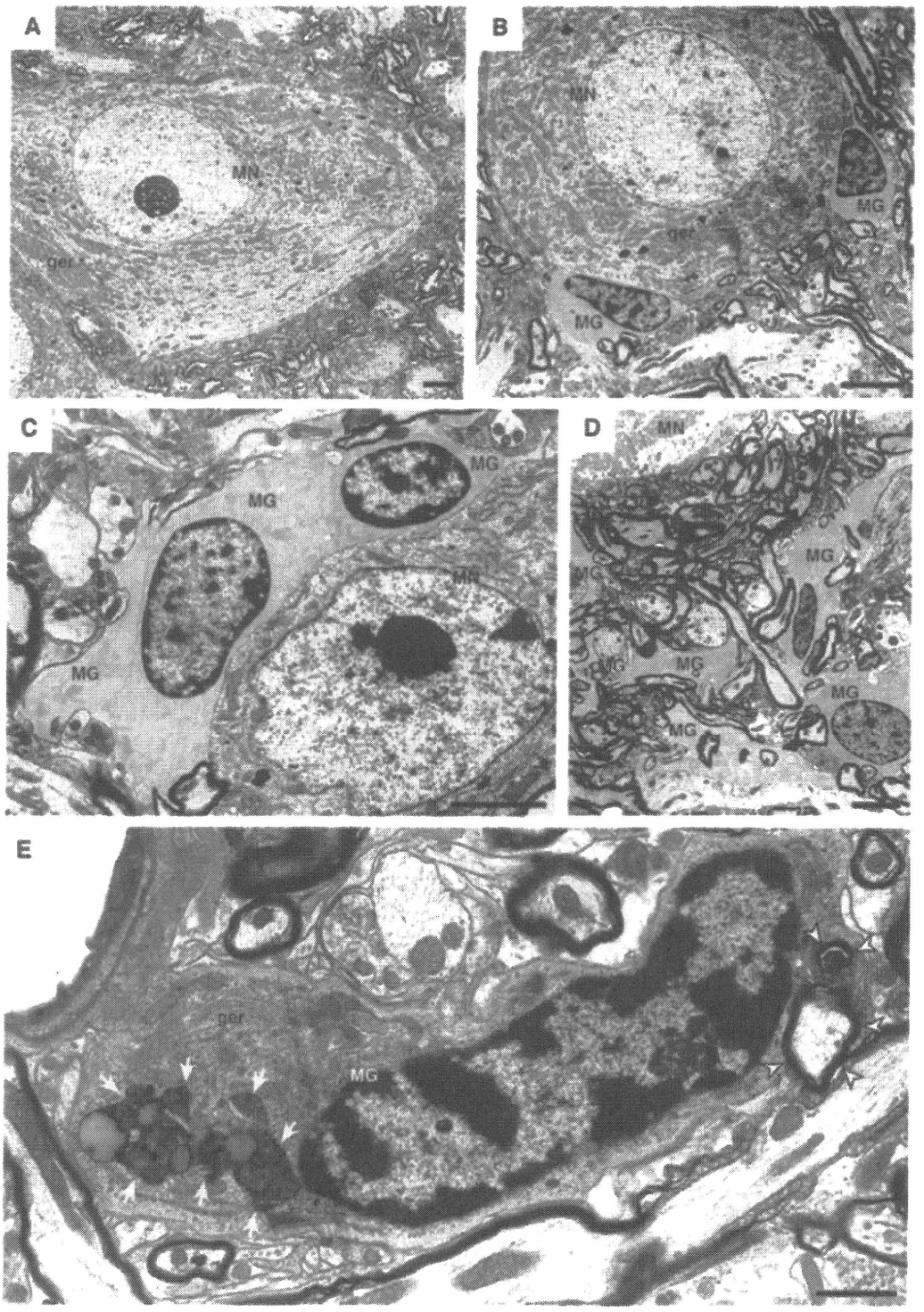

Fig. 4. Electron microscopic observation of the microglia and neuronal component in the anterior horn. **A**: In the anterior horn of wild-type rat, few microglia were attached to the somata of motoneurons (MN), and granular endoplasmic reticulum (ger) was abundant in the perikarya. **B**: In the anterior horn of the mutant $SOD1^{H46R}$ rat, several isolated microglia (MG) were attached to the somata of motoneurons that contained the granular endoplasmic reticulum abundantly and exhibited the appearance of normal morphology as early as the presymptomatic stage. **C**: The somata of mutant motoneurons with reduced granular endoplasmic reticulum and altered nucleus were surrounded by clusters of microglia as early as the presymptomatic stage. **D**: Large clusters of microglia with many processes were found among the motoneurons and surrounded the neuropils in the anterior horn of the mutant $SOD1^{H46R}$ rat as early as the presymptomatic stage. **E**: Spinal microglia at the presymptomatic stage represented an elongated nucleus harboring large clumps of chromatin beneath the nuclear envelope, and many inclusion bodies, dark lipofuscin granules (arrows), degenerating axons (arrowheads) and long cisternae of the granular endoplasmic reticulum were contained in the dark cytoplasm. Scale bars = 3 μm in A–D, 1 μm in E.

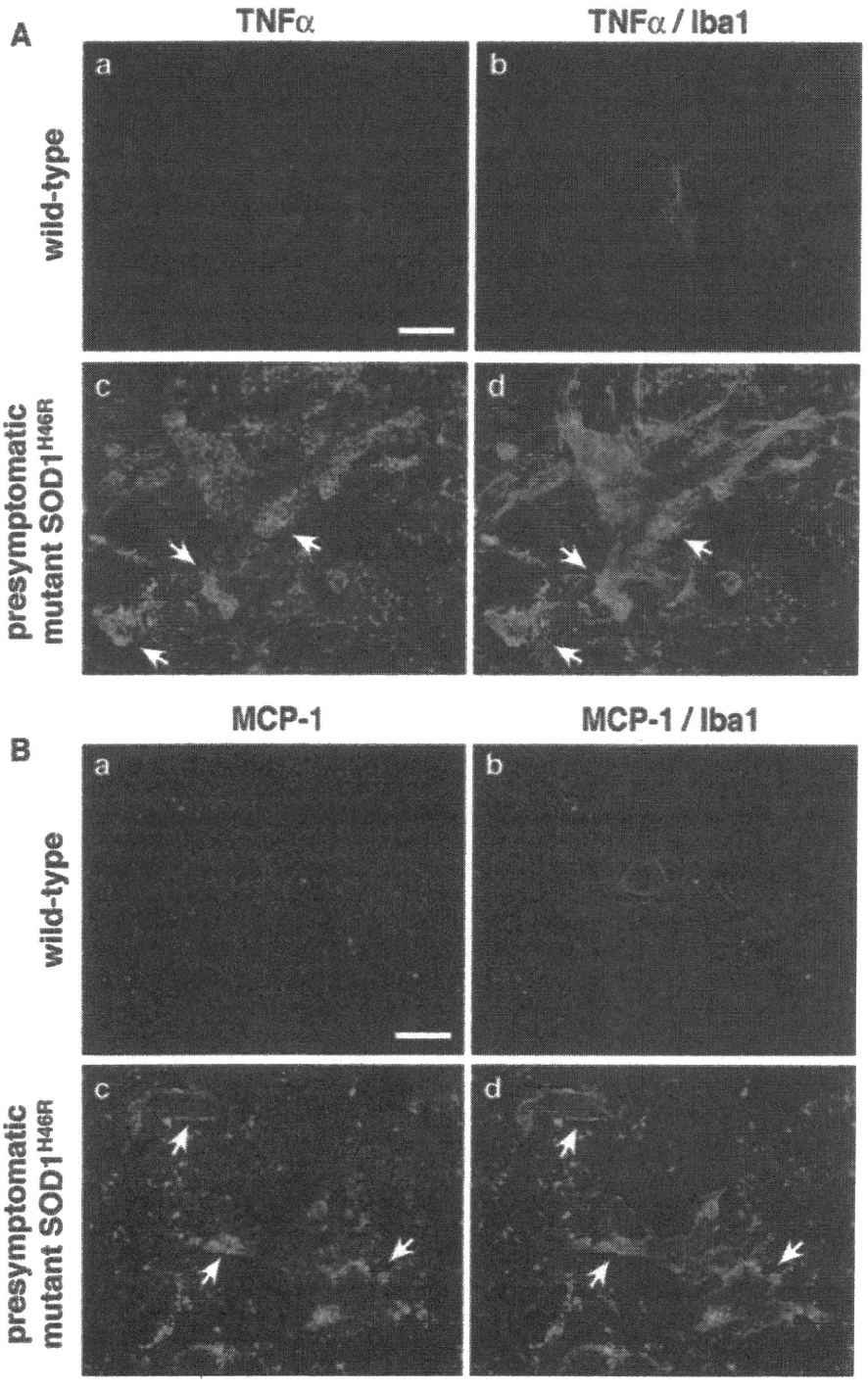

Fig. 5. Spinal cord sections of wild-type and presymptomatic mutant $SOD1^{H46R}$ rats were immunostained with anti-TNFα (green in **A**), anti-MCP-1 (green in **B**), and anti-Iba1 (red) antibodies. Microglial aggregates observed in the anterior horn of presymptomatic mutant $SOD1^{H46R}$ rats were immunoreactive for TNFα (A) and MCP-1 (B). Scale bars = 10 μm.

symptomatic mutant $SOD1^{H46R}$ rats compared with wild-type rats (Fig. 1, Supp. Info. Fig. 1B), but ChAT immunoreactivity was weaker in the motoneurons near aggregated microglia in presymptomatic mutant $SOD1^{H46R}$ rats (Fig. 2, Supp. Info. Fig. 1C). ChAT immunoreactivity has been reported to be decreased in well-preserved neurons during the early, nonadvanced stage of ALS (Kato, 1989). Previous studies have shown that motoneuronal lipid peroxidative injury occurs before the motoneuron pathology, which precedes the onset of the ultrastructural and clinical motoneuron disease (Hall et al., 1997, 1998a). We immunohistochemically confirmed that the expression of malondialdehyde, which is a marker of lipid peroxidation, was increased in the motoneurons of presymptomatic mutant $SOD1^{H46R}$ rats compared with wild-type rats (data not shown). Electron microscopy also revealed that the somata of motoneurons surrounded by aggregated microglia contained the reduced granular endoplasmic reticulum and altered nucleus (Fig. 4C). Thus, microglia might react to these neuronal changes early during ALS pathogenesis, becoming activated and forming aggregates.

We have demonstrated that the aggregated microglia observed in the lumbar spinal cord sections of presymptomatic mutant $SOD1^{H46R}$ rats were proliferative. Proliferative activity is one of the characteristic properties of activated microglia. Microglia are known to proliferate in response to macrophage colony-stimulating factor (M-CSF) and granulocyte macrophage (GM-) CSF (Giulian and Ingeman, 1988; Lee et al., 1994). The M-CSF level is reported to be elevated in the CNS of ALS patients and ALS mouse models (Henkel et al., 2004; Sargsyan et al., 2005). Therefore, in the lumbar spinal cord of presymptomatic mutant $SOD1^{H46R}$ rats, the proliferation of microglia might be induced by M-CSF, resulting in the appearance of microglial aggregates. Further studies are required to investigate whether M-CSF or any other factors induce the formation of microglial aggregates.

Our immunohistochemical and ultrastructural analyses showed that phagocytic microglia were observed in the lumbar spinal cord of presymptomatic mutant $SOD1^{H46R}$ rats. Phagocytosis by microglia is an important function for the removal of dead cells and the inhibition of content leakage from dying cells (Raivich et al., 1999; Stolzing and Grune, 2004; Neumann et al., 2009). When facial nerve neurons are damaged by the injection of toxic ricin into the facial nucleus, microglia are known to exhibit phagocytic activity in association with the removal of dead cells (Streit and Kreutzberg, 1988). On the other hand, the transection of a facial nerve does not cause neuronal cell death, and activated microglia around the facial nucleus do not exhibit any phagocytic properties (Moran and Graeber, 2004). Therefore, neuronal cell death is considered to transform microglia into phagocytic cells (Stolzing and Grune, 2004; Neumann et al., 2009). In ischemia and various neurodegenerative diseases, phagocytic microglia are thought to appear following neuronal cell loss. However, in the lumbar spinal cord sections of presymptomatic mutant $SOD1^{H46R}$ rats, the loss of motoneurons was not observed (Fig. 1A, Supp. Info. Fig. 1B), and the aggregated microglia surrounding the motoneurons exhibited phagocytic features (Figs. 3B,C, 4E). These results suggest that microglial phagocytosis occurs not only after neuronal cell death but also during the early, nonadvanced stage of neuronal cell damage.

The expression of TNFα and MCP-1 is reportedly elevated in microglia isolated from mutant $SOD1^{G93A}$ transgenic mice (Weydt et al., 2004; Sargsyan et al., 2009). We have shown that immunopositive signals for TNFα and MCP-1 were localized in the aggregated microglia (Fig. 5). In diseased CNS tissues, proinflammatory factors secreted by activated microglia are known to contribute to the regulation of microglial activation in an autocrine/paracrine manner. TNFα reportedly increases the phagocytic activity of microglia (Smith et al., 1998). Therefore, we suggest that TNFα might be involved in the transformation of activated microglia to phagocytic cells. Although the involvement of MCP-1 in the phagocytic activity of microglia is still unclear, MCP-1 has been reported to induce the chemotactic migration of microglia (Zhou et al., 2007; Deng et al., 2009). MCP-1 may regulate the recruitment of microglia to damaged neurons. In various neurodegenerative diseases, such as ALS, activated microglia are thought to influence the survival of neurons by releasing inflammatory mediators, such as nitric oxide, interleukin (IL)-1β, and IL-6 (Nakajima and Kohsaka, 2001, 2004; Sargsyan et al., 2005). TNFα has been shown to induce oxidative stress and motoneuron death in rat spinal cord (Mir et al., 2009), suggesting that TNFα might damage motoneurons and be involved in disease progression during the presymptomatic stage in ALS. On the other hand, MCP-1 is important for the recruitment of immune cells to the damaged area and reportedly provides a neuroprotective function (Eugenin et al., 2003). However, the blocking of MCP-1 function has been reported to prolong the survival of mutant SOD1 transgenic mice (Keep et al., 2001). Further studies are needed to determine whether MCP-1 has a protective or injurious effect on motoneurons during the presymptomatic stage. In the cerebrospinal fluid and CNS tissues of ALS patients and ALS animal models, various factors such as IL-6 and M-CSF have been reported to be elevated (Sargsyan et al., 2005). Therefore, further studies are needed to investigate whether these factors are expressed in aggregated microglia and whether they are involved in the promotion of motoneuronal degeneration at the presymptomatic stage.

It has been reported that the increase in activated microglia and the up-regulation of proinflammatory factors escalate in accordance with disease progression (Hall et al., 1998b; Alexianu et al., 2001; Sargsyan et al., 2005). Thus, microglia seem to play a crucial role during the late stage of disease progression. However, our results provide in vivo evidence suggesting that activated and aggregated microglia exhibit phagocytic activity and

might be involved in disease progression during the presymptomatic stage in ALS. Further studies revealing the functional properties of activated microglia during the presymptomatic stage would likely further our understanding of the role of microglia in the pathogenesis of ALS.

REFERENCES

Alexianu ME, Kozovska M, Appel SH. 2001. Immune reactivity in a mouse model of familial ALS correlates with disease progression. Neurology 57:1282–1289.

Anneser JM, Chahli C, Ince PG, Borasio GD, Shaw PJ. 2004. Glial proliferation and metabotropic glutamate receptor expression in amyotrophic lateral sclerosis. J Neuropathol Exp Neurol 63:831–840.

Aoki M, Ogasawara M, Matsubara Y, Narisawa K, Nakamura S, Itoyama Y, Abe K. 1993. Mild ALS in Japan associated with novel SOD mutation. Nat Genet 5:323–324.

Aoki M, Kato S, Nagai M, Itoyama Y. 2005. Development of a rat model of amyotrophic lateral sclerosis expressing a human SOD1 transgene. Neuropathology 25:365–370.

Beers DR, Henkel JS, Xiao Q, Zhao W, Wang J, Yen AA, Siklos L, McKercher SR, Appel SH. 2006. Wild-type microglia extend survival in PU.1 knockout mice with familial amyotrophic lateral sclerosis. Proc Natl Acad Sci U S A 103:16021–16026.

Boillee S, Vande Velde C, Cleveland DW. 2006a. ALS: a disease of motor neurons and their nonneuronal neighbors. Neuron 52:39–59.

Boillee S, Yamanaka K, Lobsiger CS, Copeland NG, Jenkins NA, Kassiotis G, Kollias G, Cleveland DW. 2006b. Onset and progression in inherited ALS determined by motor neurons and microglia. Science 312:1389–1392.

Bruijn LI, Miller TM, Cleveland DW. 2004. Unraveling the mechanisms involved in motor neuron degeneration in ALS. Annu Rev Neurosci 27:723–749.

Cereda C, Baiocchi C, Bongioanni P, Cova E, Guareschi S, Metelli MR, Rossi B, Sbalsi I, Cuccia MC, Ceroni M. 2008. TNF and sTNFR1/2 plasma levels in ALS patients. J Neuroimmunol 194:123–131.

Clement AM, Nguyen MD, Roberts EA, Garcia ML, Boillee S, Rule M, McMahon AP, Doucette W, Siwek D, Ferrante RJ, Brown RH Jr, Julien JP, Goldstein LS, Cleveland DW. 2003. Wild-type nonneuronal cells extend survival of SOD1 mutant motor neurons in ALS mice. Science 302:113–117.

Deng YY, Lu J, Ling EA, Kaur C. 2009. Monocyte chemoattractant protein-1 (MCP-1) produced via NF-kappaB signaling pathway mediates migration of amoeboid microglia in the periventricular white matter in hypoxic neonatal rats. Glia 57:604–621.

Eugenin EA, D'Aversa TG, Lopez L, Calderon TM, Berman JW. 2003. MCP-1 (CCL2) protects human neurons and astrocytes from NMDA or HIV tat induced apoptosis. J Neurochem 85:1299–1311.

Giulian D, Ingeman JE. 1988. Colony-stimulating factors as promoters of ameboid microglia. J Neurosci 8:4707–4717.

Hall ED, Oostveen JA, Andrus PK, Anderson DK, Thomas CE. 1997. Immunocytochemical method for investigating in vivo neuronal oxygen radical induced lipid peroxidation. J Neurosci Methods 76:115–122.

Hall ED, Andrus PK, Oostveen JA, Fleck TJ, Gurney ME. 1998a. Relationship of oxygen radical-induced lipid peroxidative damage to disease onset and progression in a transgenic model of familial ALS. J Neurosci Res 53:66–77.

Hall ED, Oostveen JA, Gurney ME. 1998b. Relationship of microglial and astrocytic activation to disease onset and progression in a transgenic model of familial ALS. Glia 23:249–256.

Henkel JS, Engelhardt JI, Siklos L, Simpson EP, Kim SH, Pan T, Goodman JC, Siddique T, Beers DR, Appel SH. 2004. Presence of dendritic cells, MCP-1, and activated microglia/macrophages in amyotrophic lateral sclerosis spinal cord tissue. Ann Neurol 55:221–235.

Imai Y, Ibata I, Ito D, Ohsawa K, Kohsaka S. 1996. A novel gene iba1 in the major histocompatibility complex class III region encoding an EF hand protein expressed in a monocytic lineage. Biochem Biophys Res Commun 224:855–862.

Kato T. 1989. Choline acetyltransferase activities in single spinal motor neurons from patients with amyotrophic lateral sclerosis. J Neurochem 52:636–640.

Keep M, Elmer E, Fong KS, Csiszar K. 2001. Intrathecal cyclosporin prolongs survival of late-stage ALS mice. Brain Res 894:327–331.

Lee SC, Liu W, Brosnan CF, Dickson DW. 1994. GM-CSF promotes proliferation of human fetal and adult microglia in primary cultures. Glia 12:309–318.

Lino MM, Schneider C, Caroni P. 2002. Accumulation of SOD1 mutants in postnatal motoneurons does not cause motoneuron pathology or motoneuron disease. J Neurosci 22:4825–4832.

Liu Y, Hao W, Dawson A, Liu S, Fassbender K. 2009. Expression of amyotrophic lateral sclerosis-linked SOD1 mutant increases the neurotoxic potential of microglia via TLR2. J Biol Chem 284:3691–3699.

Mattiazzi M, D'Aurelio M, Gajewski CD, Martushova K, Kiaei M, Beal MF, Manfredi G. 2002. Mutated human SOD1 causes dysfunction of oxidative phosphorylation in mitochondria of transgenic mice. J Biol Chem 277:29626–29633.

Mir M, Asensio VJ, Tolosa L, Gou-Fabregas M, Soler RM, Llado J, Olmos G. 2009. Tumor necrosis factor alpha and interferon gamma cooperatively induce oxidative stress and motoneuron death in rat spinal cord embryonic explants. Neuroscience (in press).

Moran LB, Graeber MB. 2004. The facial nerve axotomy model. Brain Res Brain Res Rev 44:154–178.

Nagai M, Aoki M, Miyoshi I, Kato M, Pasinelli P, Kasai N, Brown RH Jr, Itoyama Y. 2001. Rats expressing human cytosolic copper-zinc superoxide dismutase transgenes with amyotrophic lateral sclerosis: associated mutations develop motor neuron disease. J Neurosci 21:9246–9254.

Nakajima K, Kohsaka S. 2001. Microglia: activation and their significance in the central nervous system. J Biochem 130:169–175.

Nakajima K, Kohsaka S. 2004. Microglia: neuroprotective and neurotrophic cells in the central nervous system. Curr Drug Targets Cardiovasc Haematol Disord 4:65–84.

Neumann H, Kotter MR, Franklin RJ. 2009. Debris clearance by microglia: an essential link between degeneration and regeneration. Brain 132:288–295.

Neusch C, Bahr M, Schneider-Gold C. 2007. Glia cells in amyotrophic lateral sclerosis: new clues to understanding an old disease? Muscle Nerve 35:712–724.

Peters A, Palay SL, Webster H. 1991. The fine structure of the nervous system: neurons and their supporting cells. New York: Oxford University Press.

Pramatarova A, Laganiere J, Roussel J, Brisebois K, Rouleau GA. 2001. Neuron-specific expression of mutant superoxide dismutase 1 in transgenic mice does not lead to motor impairment. J Neurosci 21:3369–3374.

Raivich G, Bohatschek M, Kloss CU, Werner A, Jones LL, Kreutzberg GW. 1999. Neuroglial activation repertoire in the injured brain: graded response, molecular mechanisms and cues to physiological function. Brain Res Brain Res Rev 30:77–105.

Rosen DR. 1993. Mutations in Cu/Zn superoxide dismutase gene are associated with familial amyotrophic lateral sclerosis. Nature 364:362.

Rosen DR, Sapp P, O'Regan J, McKenna-Yasek D, Schlumpf KS, Haines JL, Gusella JF, Horvitz HR, Brown RH Jr. 1994. Genetic linkage analysis of familial amyotrophic lateral sclerosis using human chromosome 21 microsatellite DNA markers. Am J Med Genet 51:61–69.

Sargsyan SA, Monk PN, Shaw PJ. 2005. Microglia as potential contributors to motor neuron injury in amyotrophic lateral sclerosis. Glia 51:241–253.

Sargsyan SA, Blackburn DJ, Barber SC, Monk PN, Shaw PJ. 2009. Mutant SOD1 G93A microglia have an inflammatory phenotype and elevated production of MCP-1. Neuroreport 20:1450–1455.

Saxena S, Cabuy E, Caroni P. 2009. A role for motoneuron subtype selective ER stress in disease manifestations of FALS mice. Nat Neurosci 12:627–636.

Smith ME, van der Maesen K, Somera FP. 1998. Macrophage and microglial responses to cytokines in vitro: phagocytic activity, proteolytic enzyme release, and free radical production. J Neurosci Res 54:68–78.

Stolzing A, Grune T. 2004. Neuronal apoptotic bodies: phagocytosis and degradation by primary microglial cells. FASEB J 18:743–745.

Streit WJ, Kreutzberg GW. 1988. Response of endogenous glial cells to motor neuron degeneration induced by toxic ricin. J Comp Neurol 268:248–263.

Weydt P, Yuen EC, Ransom BR, Moller T. 2004. Increased cytotoxic potential of microglia from ALS transgenic mice. Glia 48:179–182.

Zhou Y, Ling EA, Dheen ST. 2007. Dexamethasone suppresses monocyte chemoattractant protein 1 production via mitogen activated protein kinase phosphatase 1 dependent inhibition of Jun N-terminal kinase and p38 mitogen-activated protein kinase in activated rat microglia. J Neurochem 102:667–678.

J Neuropathol Exp Neurol

Vol. 69, No. 10
October 2010
pp. 1044–1056

ORIGINAL ARTICLE

Induction of Protective Immunity by Vaccination With Wild-Type Apo Superoxide Dismutase 1 in Mutant SOD1 Transgenic Mice

Shigeko Takeuchi, MS, Noriko Fujiwara, PhD, Akemi Ido, PhD, Miki Oono, MD, Yuki Takeuchi, MD, Minako Tateno, PhD, Keiichiro Suzuki, MD, PhD, Ryosuke Takahashi, MD, PhD, Ikuo Tooyama, MD, PhD, Naoyuki Taniguchi, MD, PhD, Jean-Pierre Julien, PhD, and Makoto Urushitani, MD, PhD

Abstract

Vaccinations targeting extracellular superoxide dismutase 1 (SOD1) mutants are beneficial in mouse models of amyotrophic lateral sclerosis (ALS). Because of its misfolded nature, wild-type nonmetallated SOD1 protein (WT-apo) may have therapeutic application for vaccination of various SOD1 mutants. We compared the effects of WT-apo to those of a G93A SOD1 vaccine in low-copy G93A SOD1 transgenic mice. Both SOD1 vaccines induced antibody against G93A SOD1 and significantly delayed disease onset compared with saline/adjuvant controls. WT-apo SOD1 significantly extended the life span of vaccinated mice. The vaccines potentiated T_H2 deviation in the spinal cord as determined by the ratio of interleukin-4 to interferon-γ (IFNγ) or tumor necrosis factor and induced C1q deposition around motor neurons. Transgenic mice had abundant microglial expression of signal transducers and activators of transcription 4, an activator of transcription of IFNγ, in the spinal cord implicating IFNγ in the pathogenesis. On the other hand, the sera from G93A SOD1-vaccinated mice showed higher IFNγ or tumor necrosis factor and yielded a lower IgG1/IgG2c ratio than the sera from WT-apo–vaccinated mice. These results indicate that the T_H1/T_H2 milieu is affected by specific vaccinations and that antigenicity might counteract beneficial effects by enhancing T_H1 immunity. Thus, because of its lower T_H1 induction, WT-apo may be a therapeutic option and have broader application in ALS associated with diverse SOD1 mutations.

Key Words: Acquired immunity, Amyotrophic lateral sclerosis, Superoxide dismutase 1, Transgenic mice, Vaccination.

INTRODUCTION

Amyotrophic lateral sclerosis (ALS) is a lethal neurodegenerative disease characterized by progressive muscle weakness and wasting. Although the precise pathogenetic mechanisms of ALS remain elusive, diverse genetic mutations have been identified in familial ALS cases and are risk factors for both sporadic and familial ALS (1). Mutations in superoxide dismutase 1 (SOD1) account for 20% of familial ALS and have been determined to be the cause of motor neuron degeneration in many instances (2). Moreover, transgenic (Tg) mice carrying the human SOD1 mutation represent an excellent animal model of ALS (3). Importantly, the concept of non–cell-autonomous motor neuron death was derived from intensive analyses of mutant SOD1 Tg mice, which has had a major impact on understanding and treating not only mutant SOD1-linked ALS but also other neurodegenerative diseases such as Parkinson, Alzheimer, and Huntington diseases (4–6). There is also growing interest in the hypothesis of prion-like spreading of disease-causing proteins in such diseases (7, 8).

On the basis of our findings that chromogranin A/B may act as chaperone-like proteins to promote secretion of mutant SOD1 (9), we targeted extracellular SOD1 of G37R SOD1 Tg mice using a G93A mutant SOD1 vaccine, which resulted in a significant delay in disease onset and extension of the life span of the vaccinated mice (10). However, vaccination against high-copy G93A SOD1 (G93AGur) mice was not effective. We ascribed this failure to the extremely high expression level of the transgene. It is also possible, however, that a combination of specific antigen and the host immune response can counteract the beneficial effects of vaccination. For example, in a report testing amyloid-β (Aβ) vaccines of wild-type (WT) or various mutations linked to familial Alzheimer disease, different inflammatory responses and IgG subclasses were elicited depending on the type of Aβ vaccine used; antibody titer against Aβ in each vaccine was high overall (11). Another approach by Kutzler et al (12) using DNA vaccines encoding WT or Flemish/Dutch mutant Aβ showed greater antigenicity

From the Molecular Neuroscience Research Center (ST, AI, MO, IT, MU), Shiga University of Medical Science, Shiga; Department of Biochemistry (NF, YT, KS), Hyogo College of Medicine, Hyogo; Department of Peripheral Nervous System Research (MT), National Institute of Neuroscience, National Center of Neurology and Psychiatry, Tokyo, Japan; Department of Psychiatry and Neuroscience (J-PJ), Research Centre of CHUQ, Laval University, Quebec, Canada; Department of Disease Glycomics (Seikagaku Corporation) (NT), The Institute of Scientific and Industrial Research, Osaka University, Osaka; Systems Glycobiology Group (NT), Disease Glycomics Team, Advanced Science Institute, RIKEN, Saitama; and Department of Neurology (MO, RT), Kyoto University, Kyoto, Japan.

Send correspondence and reprint requests to: Makoto Urushitani, MD, PhD, Unit for Neurobiology and Therapeutics, Molecular Neuroscience Research Center, Shiga University of Medical Science; Shiga, Japan; E-mail: uru@belle.shiga-med.ac.jp

This study was funded by the Japan Society for the Promotion of Science, Japan Health and Labour Science Research Grants, Japan ALS Association, and Takeda Science Foundation.

Supplemental digital content is available for this article. Direct URL citations appear in the printed text and are provided in the HTML and PDF versions of this article on the journal's Web site (www.jneuropath.com).

and T_H1 immune response to the mutant than the WT Aβ peptide. The T_H1 cytokines tumor necrosis factor (TNF) and interferon-γ (IFNγ) are implicated in motor neuron degeneration in ALS (13, 14), whereas the T_H2 cytokine interleukin-4 (IL-4) provides protective immunity to prevent motor neuron death (15). Moreover, T cells are present in the spinal cord of ALS patients (16), and circulating $CD4^+$ T cells affect the disease course of ALS model mice (17–19). In particular, $CD4^+$ T cells stimulate astrocytes or microglia to express neuroprotective molecules including glutamate transporter or insulin-like growth factor 1 (IGF-1) (17). The effects of different types of acquired immunity induced by different vaccines on the therapeutic outcome, however, have not been systematically studied.

More than 120 mutations in SOD1 covering overall domains have been reported. Therefore, it would be desirable to develop a vaccine that is effective and not dependent on thespecific SOD1 mutation associated with the disorder. One approach is to target the core domain of the molecule, i.e. the dimer interface (20). Another approach is to use apo WT SOD1, the molecular behavior of which is similar to that of the mutant molecules (21, 22). We previously reported that wild-type (WT) SOD1 with posttranslational modifications, including oxidative modification, gains properties similar to those of mutant SOD1 (10). Other reports show possible involvement of WT SOD1 in the pathogenesis of sporadic ALS. For example WT SOD1 has been detected in cytoplasmic aggregates and abnormal dimer formations have been reported in the spinal cord of sporadic ALS patients (23, 24). Therefore, the development of SOD1 vaccine based on the WT sequence deserves investigation because of its potential broad application not only in mutant SOD1-associated but also in sporadic ALS.

Here, we compared the effects of G93A-apo SOD1 and WT-apo SOD1 vaccines on the survival and the life span of low-copy G93A SOD1 Tg mice ($G93AGur^{dl}$) and analyzed the relationships to the cellular and humoral immune responses elicited by the vaccinations.

MATERIALS AND METHODS

Materials

All chemicals were obtained from Nacalai Tesque, Inc (Kyoto, Japan), unless specified otherwise, and were of the highest grade available.

Purification of Recombinant SOD1 From *Escherichia coli*

Recombinant human WT and gly93ala (G93A) mutant SOD1 were produced in *Escherichia coli* according to a previous report (22). The eluates were dialyzed against endotoxin-free saline and subsequently stored at −80°C until use. Metallation of the recombinant SOD1 was performed as previously described (22). The metallated and nonmetallated SOD1s were designated as holo-SOD1s and apo-SOD1s, respectively. Control monomeric SOD1 was prepared by treating recombinant human SOD1 chemically modified with 2-mercaptoethanol at Cys111 (2-ME-SOD1 (25). The purity of the recombinant protein was assessed by sodium dodecyl sulfate-polyacrylamide gel electrophoresis (SDS-PAGE) and gel staining with Coomassie brilliant blue. Details are provided in Methods, Supplemental Digital Content 1, http://links.lww.com/NEN/A178.

Molecular-Size Filtration Chromatography

A total of 100 μL of SOD1 proteins (2–3 mg/mL) in phosphate-buffered saline (PBS) (−) were applied to a molecular-size filtration high-performance liquid chromatography (AKTA Explorer 10S) at a flow rate of 0.5 mL/min on Superdex 75 10/30 (GE Healthcare, Piscataway, NJ) equilibrated with 50 mmol/L sodium phosphate buffer containing 0.15 mol/L NaCl, pH 7.4. The calibration of the column for the estimation of molecular weight was performed using bovine serum albumin (Intergen, Milford, MA), ovalbumin (GE Healthcare), and *E. coli* thioredoxin (Promega, Madison, WI), as protein standards.

Animal Experiments

Tg mice harboring human G93A SOD1 (B6SJL-TgN[SOD1-G93A]1Gur, hSOD1G93A; Jackson Laboratory, Bar Harbor, ME) were backcrossed with C57BL/6 strain for more than 20 generations ($G93AGur^{dl}$). $G93AGur^{dl}$ mice were vaccinated with apo recombinant human SOD1 (WT or G93A) or human erythrocyte-derived SOD1 (Sigma) with Monophosphoryl Lipid A- Trehalose Dicorynomycolate (MPL-TDM; Ribi) adjuvant, as previously reported (10). From day 100, motor performance was evaluated for onset of decreased rotarod retention time (Muromachi, Tokyo, Japan) and body weight (BW) change to determine the time of onset (Methods, Supplemental Digital Content 1, http://links.lww.com/NEN/A178). The data for the survival and onset were analyzed by Kaplan-Meyer curve and log-rank test using Prism software (GraphPad, La Jolla, CA).

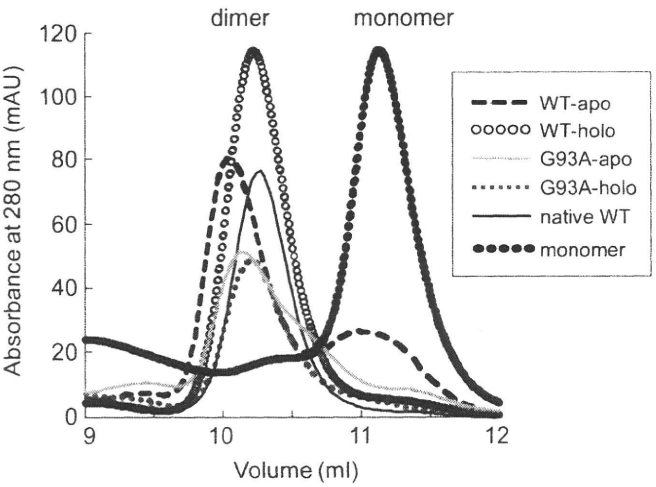

FIGURE 1. Characterization of recombinant human G93A or wild-type (WT)-apo superoxide dismutase 1 (SOD1) proteins. The chromatogram profile of SOD1 proteins separated with a gel filtration column. The native WT-SOD1, apo-WT, apo-G93A, holo-WT, holo-G93A, and monomeric SOD1, were eluted on Superdex 75 column. The elution profiles were monitored by the absorbance change at 280 nm. apo- indicates nonmetallated; holo-, metallated.